Application of spectral linear mixing to rock slabs analyses at various scales using Ma_Miss BreadBoard instrument

Simone De Angelis[1], Paola Manzari[1], Maria Cristina De Sanctis[1], Francesca Altieri[1], Cristian Carli[1], Giovanna Agrosì[2]

[1] *Institute for Space Astrophysics and Planetology, INAF-IAPS, via Fosso del Cavaliere, 100, 00133 - Rome (Italy)*
[2] *University of Bari "Aldo Moro", Department of Earth and Geoenvironmental Sciences, via Orabona, 4, 70125 – Bari (Italy)*

**Corresponding author: Simone De Angelis; email: simone.deangelis@iaps.inaf.it, tel: +39-06-49934083*

Abstract

Focus of this work is the analysis of rock slabs by means of the Ma_Miss BreadBoard instrument. Ma_Miss (Mars Multispectral Imager for Subsurface Studies, Coradini et al., 2010; De Sanctis et al., 2017) is the miniaturized imaging spectrometer onboard the ESA Exomars 2020 mission.

Here we report the results of the analysis carried out on rock slabs using the Ma_Miss breadboard (BB) (De Angelis et al., 2014; 2015) and a Spectro-Goniometer (SPG). The samples are three volcanic rocks (from the Aeolian Islands and Montiferru volcanoes, Italy) and two carbonate rocks (from Central Apennines, Italy). Visible and near infrared spectroscopic characterization has been first performed on all the samples with a Spectro-goniometer (SPG). Successively, higher spatial resolution spectra were acquired with the Ma_Miss BB setup in each of the areas analyzed with the SPG.

We compared the spectra of the same areas of the slabs, acquired with SPG and Ma_Miss BB. Three different analysis approaches have been performed on the spectra: arithmetical averaging of the spectra, linear mixing of reflectances and linear mixing of Single Scattering Albedoes (using Hapke model). The comparison shows that: (i) Ma_Miss instrument has great capabilities for the investigation of rock surfaces with high detail; a large number of different mineralogical phases can be recognized thanks to Ma_Miss high resolution within each millimeter-sized analyzed area; (ii) the agreement with SPG spectra is excellent especially when linear mixing is applied for the convolution of Ma_Miss BB spectra.

1. Introduction

The Ma_Miss instrument (Coradini et al., 2001, De Sanctis et al., 2017) onboard the ExoMars-2020 Rover mission (Vago et al., 2007; 2013) will perform detailed spectroscopic

investigation of the Martian shallow subsurface, in the Visible and Near-Infrared spectral range (0.4-2.2-μm). Many different mineral classes can be identified by spectral signatures occurring in this range, such as Fe-bearing silicates, OH-bearing phyllosilicates and clays, sulfates and iron-oxides, widely observed on the surface of Mars (see Ehlmann and Edwards 2014, for a recent review of Martian mineralogy). The surface of Mars is mainly constituted by mafic silicates (clino- and ortho-pyroxenes and olivine) and plagioclase, as constituents of volcanic rocks of basaltic composition (e.g. Bibring et al., 2005; Poulet et al., 2007; Ehlmann and Edwards 2014). Hydrated minerals (phyllosilicates and sulfates) have been observed by both OMEGA (Observatoire pour la Minéralogie, l'Eau, les Glaces et l'Activité)/Mars Express and CRISM (Compact Reconnaissance Imaging Spectrometer for Mars)/Mars Reconnaissance Orbiter remote-sensing instruments and also by Mars Science Laboratory onboard Curiosity rover (e.g Bibring et al., 2005; Murchie et al., 2009; Vaniman et al., 2014). Various types of carbonates have been detected from the orbiting instrument CRISM/MRO (e.g Niles et al., 2013). In addition to mineral phases, water and carbon dioxide ice mixtures have been identified in polar caps (e.g Bibring et al., 2004, Langevin et al., 2005, 2007) and water ice is likely to be present in the subsurface (Boynton et al., 2002).

Several works in the last decade have focused on spectroscopic analyses of rocks in the form of coarse grains, fragments or slabs, with relevance for planetary surfaces investigations and remote sensing data interpretation. Differences in spectra of powders and rock slabs are well known (see for example Harloff & Arnold, 2001) and mainly concern different spectral slopes, number of absorption features and spectral contrast. Longhi et al. (2001, 2004) analyzed in the VNIR (0.4-2.5 μm) metamorphic rocks slabs from Madagascar (quartzites, micaschists, marbles, gneisses). They suggested the concept of *spectrofacies,* as a combination of several absorption features; variation of absorption patterns are diagnostic of different types of rocks. In another work Sgavetti et al. (2006) again point to the use of the concept of *spectrofacies* for spectral classification of mafic and metamorphic rocks.

Pompilio et al. (2007) investigated bulk mafic cumulate rock samples, separated minerals extracted from the bulk as endmembers and their mixtures. The main difference arising between particulate minerals/synthetic mixtures and bulk rocks slabs is that, in the case of rock slabs, the constituents interact in a complex manner. Spectral trends and correlations with mineral chemistry are strongly influenced by the presence in bulk samples of one or more spectrally active dominant species (Longhi et al., 2004; Sgavetti et al., 2006; Pompilio et al., 2007). Isaacson et al. (2011) also report a similar work concerning combined investigation of both bulk (rock slabs) and extracted mineral separates, focusing on lunar basalts and computing linear mixing of mineral endmembers.

Other authors focused on the study of rock slabs of ultramafic to plagioclase cumulates and basalts (Carli, 2009; Carli and Sgavetti, 2011; Carli et al., 2014), analyzing the spectral differences due to intrusive/effusive textural properties. Moreover, an important factor controlling the spectral shape and reducing the albedo and spectral contrast, is given by the number of FeO-bearing constituents within a rock, more than the absolute total FeO content (Carli and Sgavetti, 2011).

In a recent work Gurgurewicz et al. (2015) analyzed basaltic rock slabs from cold and hot arid environments, with the aim to investigate spectral effects produced by weathering and application to Mars, and concluding that rock slabs do not fully report spectral information about the alteration history and paleo-environment conditions.

In two previous papers we demonstrated how Ma_Miss is able to discriminate between different types of particulate minerals and rocks, discriminating between different grain sizes and retrieving information about spectral parameters (De Angelis et al., 2014; 2015). Ma_Miss will observe with high spatial resolution (120 μm) the borehole excavated by the Drill in the subsurface at different depths, from about 0.3 m down to a maximum of 2 m. This high spatial resolution is comparable with typical grain sizes in the regolith and can be much smaller than the characteristic layer size in a stratigraphic column; Cousin et al. (2015) for example report that coarse grains (>500 μm) constitute about half of the soils observed at Gale Crater. Thus Ma_Miss observations will allow reconstructing the stratigraphy of the observed borehole column. Depending on the material strength of the excavated column, powder-like or slab-like surfaces will be observed by the instrument. Assuming a slab-like texture of the excavated borehole, Ma_Miss will allow retrieving information both about differences in the stratigraphy and mineralogical heterogeneity at a sub-millimeter scale level.

In order to estimate and validate Ma_Miss setup performances when observing slab-like rocks surfaces, a second instrument, the Spectro-Goniometer, having a much larger spatial resolution (6 mm) has been used. Methodologies and experimental setup are described in section 2. Rock samples used in this work, three volcanic (STR72, FOR5, MFEB1) and two carbonate samples (CAL1, GPR18), are described in section 3; before spectroscopic measurements, the samples were characterized in terms of chemical and mineralogical composition, by means of X-Ray Fluorescence and X-Ray Powder Diffraction techniques (section 3). Several areas have been then observed with the Spectro-Goniometer (SPG) on each rock surface. Each area corresponds to the SPG spatial resolution of 6 mm and thus to a single SPG spectrum. Subsequently, given the much higher spatial resolution of Ma_MISS, 10 high-resolution spectra have been acquired with Ma_Miss setup in each of these areas (section 4).

The comparison of Ma_MISS spectra with measurements performed with the Spectro-Goniometer (SPG), having a much larger spatial resolution, implies the use of statistical methods, especially if we are observing a rock slab with mm-sized surface heterogeneity. A first simple method used to retrieve the SPG spectra is to average all Ma_Miss spectra acquired within a comparable area; this method is used in section 4.4. A second method is based on the linear mixing of reflectance spectra. Three endmembers are extracted among the ten spectra acquired with Ma_Miss within each area, and a linear combination of these ones is computed and optimized to match the corresponding SPG spectrum (section 4.5). The linear mixing of reflectance spectra results in a better final matching with the SPG spectrum; nevertheless this approach is rigorously valid if the mixing scale is macroscopic (Mustard and Pieters, 1987). A third approach concerns the linear mixing of Single-Scattering Albedo (SSA) spectra, for which a linear behavior is expected in case of microscopic mixing scale (Hapke, 1981; Mustard and Pieters, 1987); this third method is described in section 4.6.

2. Experimental setup

2.1 Ma_Miss Breadboard setup

The Laboratory BreadBoard setup in use at INAF-IAPS (described in detail in De Angelis et al., 2014) consists of the main optical subsystems of the Ma_Miss instrument (Coradini et al., 2001; Preti et al., 2011) except for the spectrometer. The illumination source is a 5W miniaturized lamp integrated within the instrument. A bundle of optical fibers carries the light from the lamp to the Optical Head, which consists of several miniaturized mirrors and acts to focus the light on the external target. The light is focused through a sapphire window on the target, at a distance of 0.6 mm; then the scattered light is recollected by the same Optical Head, and an optical fiber carries the signal to a spectrometer. In this setup the BreadBoard is coupled with a FieldSpec Pro, which operates in the 0.35-2.5 μm range. The Ma_Miss instrument will nominally operate in the 0.4-2.2 μm range. The illuminated area on the target is 1 mm, while the spatial resolution is about 0.12 mm.

2.2 Spectro-Goniometer setup

This setup (in use at INAF-IAPS) consists of the Spectro-photometer FieldSpec Pro coupled with a mechanical goniometer, which permits to vary phase angles with a minimum of 30°. Illumination and emission angles used with this setup are i=30° and e=0°, respectively. The light source is a Quartz Tungsten Halogen (QTH) lamp (power 84W). The illuminated and sensible area onto the target is about 6 mm. The main differences between these two setups have, in terms of spatial resolution, illumination conditions and other factors, have already been described in De Angelis et al. (2014).

2.3 Optical microscopy

All the samples have been analyzed by optical microscopy. The microscope used is a Nikon SMZ 800, equipped with an ED Plan 1.5X WD 45 Nikon objective, C-W10X/22 Nikon oculars, and light source Schott, in use at IAPS-INAF. Microscopy investigation has been carried out inside each single 6-mm sized area observed with the Spectro-Goniometer. Samples have been observed in reflection mode in the form of slabs. Magnifications in the range 1-6.3X have been used among samples depending on particular features (see figs 2 to 6 in section 3). This has been done with the aim of searching and discriminating, within each area observed with the Spectro-Goniometer, grains and features to be successively analyzed with Ma_MISS setup.

2.4 XRF and XRPD analyses

X-Ray Fluorescence (XRF) and X-Ray Powder Diffraction (XRPD) analyses have been carried out at the University of Bari on all samples except the San Bartolo Lava (STR72) volcanic sample, whose analyses were published in Laiolo & Cigolini (2006) (see section 3). Both XRF and XRPD analyses have been performed on powders, obtained from volumes that were representative of whole slabs. XRF analyses have been performed on the two volcanic samples (FOR5 and MFEB1) in order to retrieve major oxide elements composition, while XRD has been performed on the two carbonate samples (CAL1 and GPR18) in order to retrieve mineralogical phases.

Before XRF analyses the samples have been ground with planetary mill Fritsch Pulverisette 7 and ZrO mortars, using four 2-minutes cycles at 300 Hz. Five grams of each sample have been mixed with 2 ml of Elvacite (15% in acetone), and this has been mixed with 5 grams of H_2BO_3 in an aluminum capsule. Pellets have been finally produced pressing this mixture at 25 tons. Analyses have been conducted on pellets using a WDXRF Rigaku Supermini 200 spectrometer with Pd source (50 kV, 4 mA, 200 W) in vacuum. Siliceous rocks standards from CNRS SARM GRPG Paris have been used for calibration. For XRPD analyses an Empyrean Panalytical Diffratometer has been used, with operating conditions 40 kV and 40 mA and CuKα radiation as source. Bragg- Brentano geometry was used. Sample stage was a flat specimen holder. The incident beam path was given by: Soller slits 0.02 rad, fixed incident beam mask 10 mm, anti-scatter slit ½°, divergence slits ¼°. The diffracted beam path was characterized by: anti-scatter slits 7.5 mm; Soller slits 0.02 rad, large beta filter-Nickel detector: PIXcel3D. A phase quantification of mineralogical composition was obtained using the software HighScore Plus™ (Panalytical).

3. Samples characterization

Five samples have been analyzed, in the form of slabs and representative powders. Three of them are volcanic samples, while the other two are carbonates. X-Ray Fluorescence spectroscopy has been performed on two volcanic samples (MFEB1 and FOR5) while X-Ray Diffraction has been performed on the carbonates (CAL1 and GPR18) at the University of Bari (Italy). In the following section the samples are described.

3.1 Macroscopic description and XRF/XRD analyses

3.1.1 San Bartolo lava (STR72)

This sample is a lava from Stromboli (Aeolian arc, Sicily/Italy). The rock is characterized by a very dark groundmass with fine porphyritic texture (fig.1A). Few small vesicles characterize the rock surface. San Bartolo lavas are characterized by a high porphyrity index (40-45 %), with plagioclase being the most abundant phase, plus clinopyroxene, olivine and orthopyroxene; accessory phases are constituted by titano-magnetite and apatite (Laiolo and Cigolini, 2006). Phenocrysts of plagioclases (anorthitic to labradoritic), olivine (mainly micro-

phenocrysts), clino- and ortho-pyroxenes and opaque minerals (oxides, titaniferous magnetite) are present. Moreover San Bartolo lavas also contain mafic/ultramafic xenoliths with gabbroic, gabbro-noritic and grabbro-anorthositic compositions. This lava can be classified as porphyritic high-K calc-alkaline basalt (Laiolo and Cigolini, 2006), with SiO_2, 52.60 wt%; Na_2O+K_2O, 3.86 wt% (Peccerillo et al., 2013).

3.1.2 Lava from Montiferru/Bonarcado (MFEB1)

The rock has been sampled in the Montiferru volcanic region (Abbasanta Plateau, Sardinia/Italy), within a unit that belongs to the Plio-Pleistocene alkaline transitional, and sub-alkaline volcanic cycle (0.14-5.3 Myr) characterized by alkaline basalts/basanites/trachybasalts. It is characterized by fine grey porphyritic texture (fig.1B), with visible phenocrysts of olivine, plagioclase and iron oxides. A great number of large vesicles also characterize the sample, indicating that it is an intermediate volcanic rock which retained large quantity of gas. XRF analyses show that this sample has SiO_2 content of 50.9% and an alkali content of Na_2O+K_2O=8.3% (phonolitic tephrite). Normative calculations suggest that the sample has a mineralogical composition given essentially by feldspar (plagioclase 63 wt%, orthoclase 22 wt%) and olivine (8 wt%). Accessory minerals are ilmenite (3 wt%), nepheline and other oxides.

3.1.3 Lava from Fordongianus (FOR5)

The sample derives from Montiferru volcanic region (Sardinia/Italy), within a unit defined by intermediate/acidic rocks. The ground mass has a pink coloured, fine and porphyritic texture (fig.1C). Some quartz and feldspar phenocrysts and large lithic fragments are embedded within the groundmass. The sample also shows few small vesicles and signs of weathering and aqueous alteration. XRF analyses show that this sample has an SiO_2 content of 65.1% and an alkali content of Na_2O+K_2O=8.5% (trachy-dacite). Normative mineralogical composition is constituted by feldspar (plagioclase 53 wt%, orthoclase 23 wt%), quartz (16 wt%), pyroxene (hypersthene 6 wt%) plus minor magnetite, ilmenite and corundum.

3.1.4 Red micritic limestone (CAL1)

This limestone ("*scaglia rossa*") derives from Apennines near Gubbio (Umbria/Italy), from a unit at the Cretaceous-Paleogene (K-T) limit (Mesozoic-Cenozoic era transition; Lowrie and Alvarez, 1977; Alvarez 2009); the sample is typical of deep-sea environment and hot-tropical climate. Optical observations show that the rock is characterized by red color likely due to the presence of iron oxides and/or hydroxides (fig.1D); very fine, sub-micron grain size texture and several grey veins. These veins can be due to percolation of fluids from which recrystallized calcite crystals, that intersect the rock matrix. XRPD analyses on powder reveal

234 that the mineralogical composition consists mainly of calcite (96%) and quartz (4%); the
235 amounts of minerals responsible of reddish color of the studied sample are below the
236 detection limit of diffractometer (1%).

237

238 ### *3.1.5 Limestone from Mt Ernici (GPR18)*

239 This sample derives from Apennines / Ernici Mountains (Lazio/Italy) (fig.1E). It is
240 characterized by very fine sub-micron grain size matrix, with substantial surface homogeneity
241 and absence of clasts. XRD analysis on this (powdered) sample show that it is composed
242 essentially by 92% dolomite [$CaMg(CO_3)_2$] with 8% ankerite [$Ca(Fe^{2+},Mg,Mn)(CO_3)_2$].

243

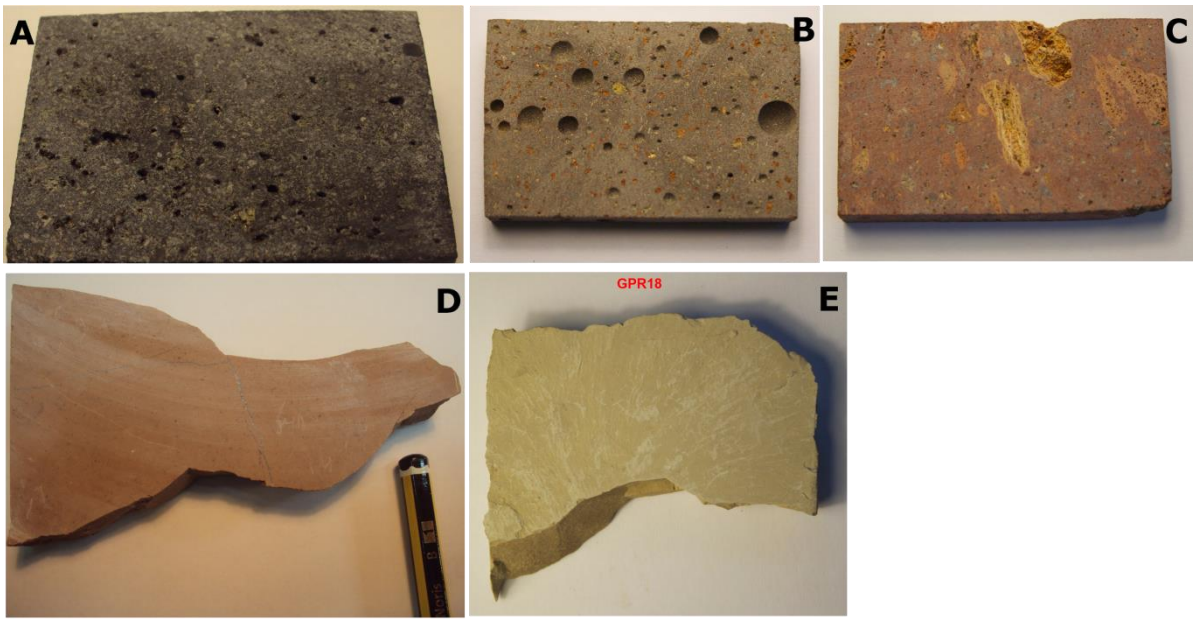

244

245

246 *Fig.1. Analyzed samples. A: San Bartolo Lava (STR72). B: Montiferru/Bonarcado lava (MFEB1). C:*
247 *Fordongianus sample (FOR5). D: Red micritic limestone (CAL1). E: limestone from Mt Ernici*
248 *(GPR18).*

249

250

251 ## 3.2 Analyses by optical microscopy

252 ### *3.2.1 San Bartolo lava (STR72)*

253 Some images acquired with the microscope from this sample are in fig.2. In the image of fig.2A
254 a phenocryst of olivine, green hexagonal section, about 1x2 mm in the left center, is evident;
255 plagioclase crystals and vesicles are also visible; plagioclase phenocrysts appear in the form of
256 laths and euhedral-subhedral crystals, sometimes with sieve texture. Pyroxenes, iron oxides

and opaques constitute the dark groundmass. In fig. 2B and 2C olivine (green crystal about 1x2 mm in the left center), oxides and plagioclases are embedded within the groundmass. In fig.2D a black inclusion, about 2x3 mm in size (likely magnetite or ilmenite or a glassy xenolith) is evident.

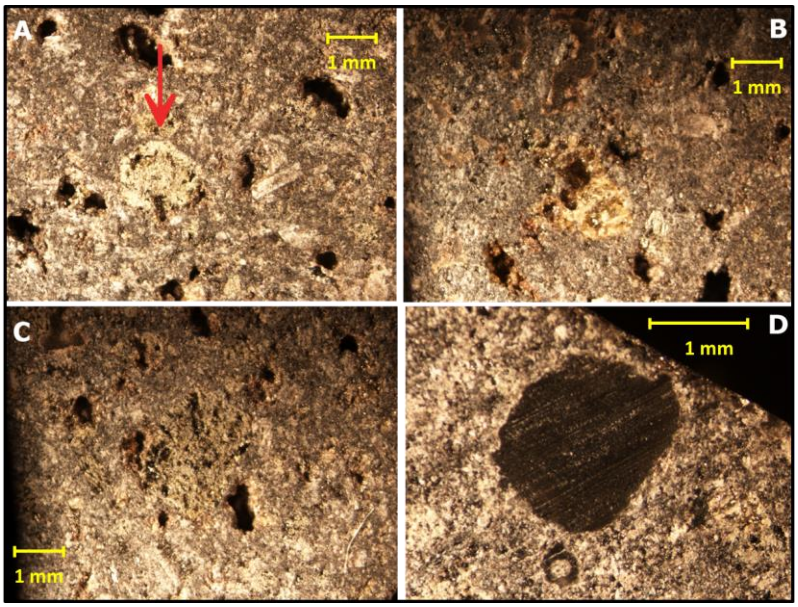

Fig.2. Microimages of San Bartolo lava's (STR72) sample. Observations under optical microscope performed on rocks surfaces in reflected light. Magnifications used are: A,B,C = 1X. D = 2X. The red arrow in 2A frame indicates the green hexagonal crystal (likely olivine).

3.2.2 Lava from Montiferru/Bonarcado (MFEB1)

In fig.3 optical microscopy images acquired in reflection mode from the Montiferru lava are shown. Several vesicles are evident in all frames. Millimeter-sized feldspars and plagioclase crystals are visible in frames A, B and C. Plagioclases phenocrysts occur in the form of white laths. Numerous reddish concretions, likely constituted by iron oxides/hydroxides occur on the rock surface. Alkali basalts occurring in these lava flows (*BD unit* described in Fedele et al., 2007) are characterized by a porphyrity index of 25-30 % and by the common presence of altered iddingsitised olivine (reddish concretions in Fig.3). The groundmass has a very fine and dark texture, substantially made of pyroxenes with plagioclase crystals.

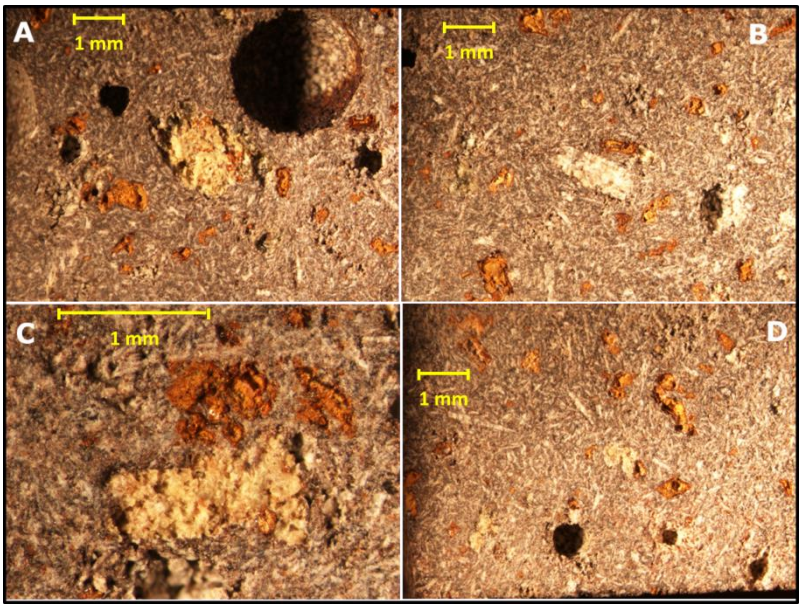

Fig.3. Microimages of Montiferru/Bonarcado (MFEB1) sample. Observations under optical microscope performed on rocks surfaces in reflection light. Magnifications used are: A,B,D = 1X. C = 3X.

3.2.3 Lava from Fordongianus (FOR5)

Optical microscope images relative to volcanic FOR5 sample are in fig.4. The pink-red groundmass is characterized by very fine and vesicular cryptocrystalline texture. Plagioclase and numerous millimetric to sub-millimetric quartz crystals are visible in fig.4A. Embedded in the matrix are also millimetric pink-orange feldspar phenocrysts and iron oxide crystals. Often iron oxides/hydroxides and anhedral quartz crystals have grown and filled inside vesicles.

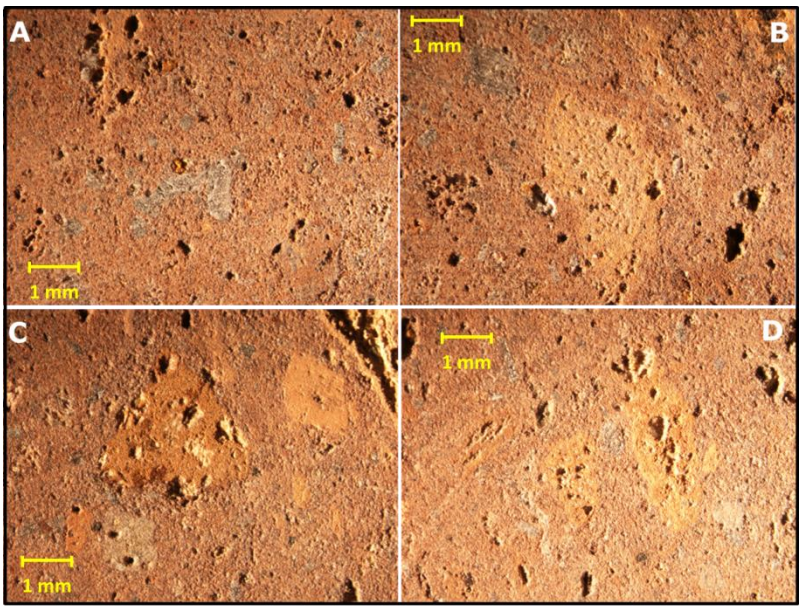

Fig.4. Microimages of Montiferru/Fordongianus (FOR5) sample. Observations under optical microscope performed on rocks surfaces in reflection light. Magnifications used are: A,B,C,D = 1X.

3.2.4 Red micritic limestone (CAL1)

In fig.5 images acquired on the red micritic limestone (Scaglia Rossa, Lowrie and Alvarez, 1977; Alvarez, 2009) are shown. The typical dimension of the calcite grains is <10 microns. Sub-millimeter hematite and magnetite grains, present in this sample (Lowrie and Alvarez, 1977), are visible especially in fig.5B, together with microfossils (about 100 micrometers in size). This *scaglia rossa* sample is a pelagic sediment, and is composed essentially by calcareous plankton (calcareous nannofossils and planktonic foraminifera, Alvarez, 2009; Cita et al., 2005). In fig.5B-D two veins filled with calcite crystals are visible.

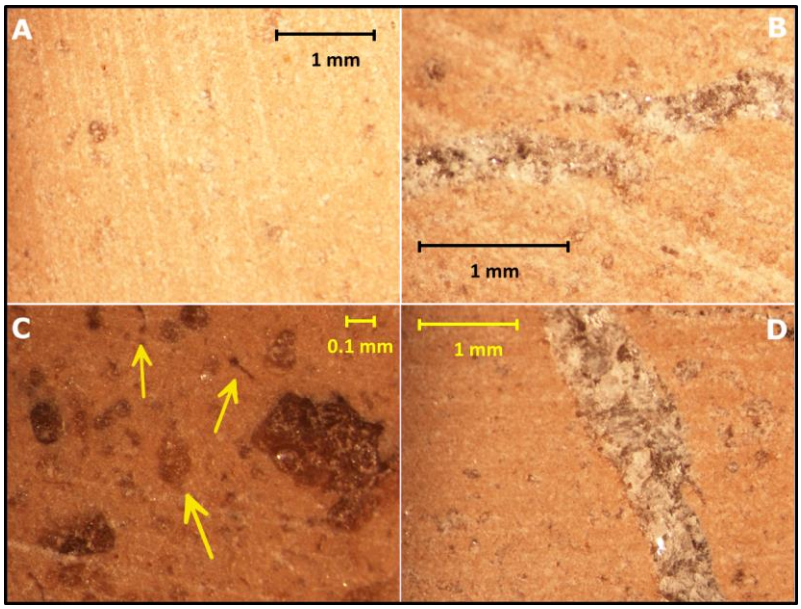

Fig.5. Microimages of the sample from Umbria/Apennines (CAL1). Observation under optical microscope performed on rocks surfaces in reflection light. Magnifications used are: A = 2X. B = 3X. C = 5X. D = 2X. Yellow arrows in frame 5C indicate nanofossils.

3.2.5 Limestone from Mt Ernici (GPR18)

A high level of surface homogeneity characterizes the images acquired from this sample, obtained at different values of magnification (fig.6). The dimension of the grains is of the order of 10 micrometers. We note the absence of clasts, inclusions or crystals of size greater than few tens of micrometers.

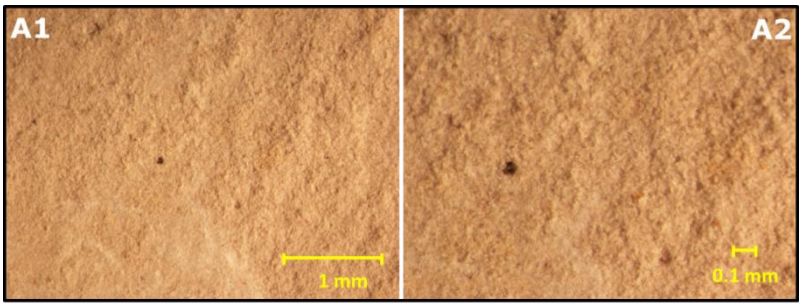

Fig.6. Microimages of the sample from Mt Ernici/Apennines (GPR18). Observations under optical microscope performed on rocks surfaces in reflection light. A1 = 2X. A2 = 4X.

4. Results: spectral analyses

All samples have been first analyzed with the SPG setup, and subsequently with the Ma_MISS BB setup. For each sample, several areas on the surface have been analyzed with the SPG, each area corresponding to the instrumental acquisition area of 6 mm. Then the BB setup has been used to acquire spectra with higher spatial resolution (120 μm of spatial resolution): thus 10 spectra in different positions have been acquired with the BB setup, inside each previous SPG area. In the following sections, the measurements will be described separately and then compared with different methods.

4.1 Measurements with Spectro-Goniometer

Spectra acquired with the Spectro-Goniometer setup are in fig.7 for all samples (I to V). In all cases the area of the spot corresponding to one spectrum is much bigger than the typical size of mineral crystals and grains which are embedded in the surface matrix.

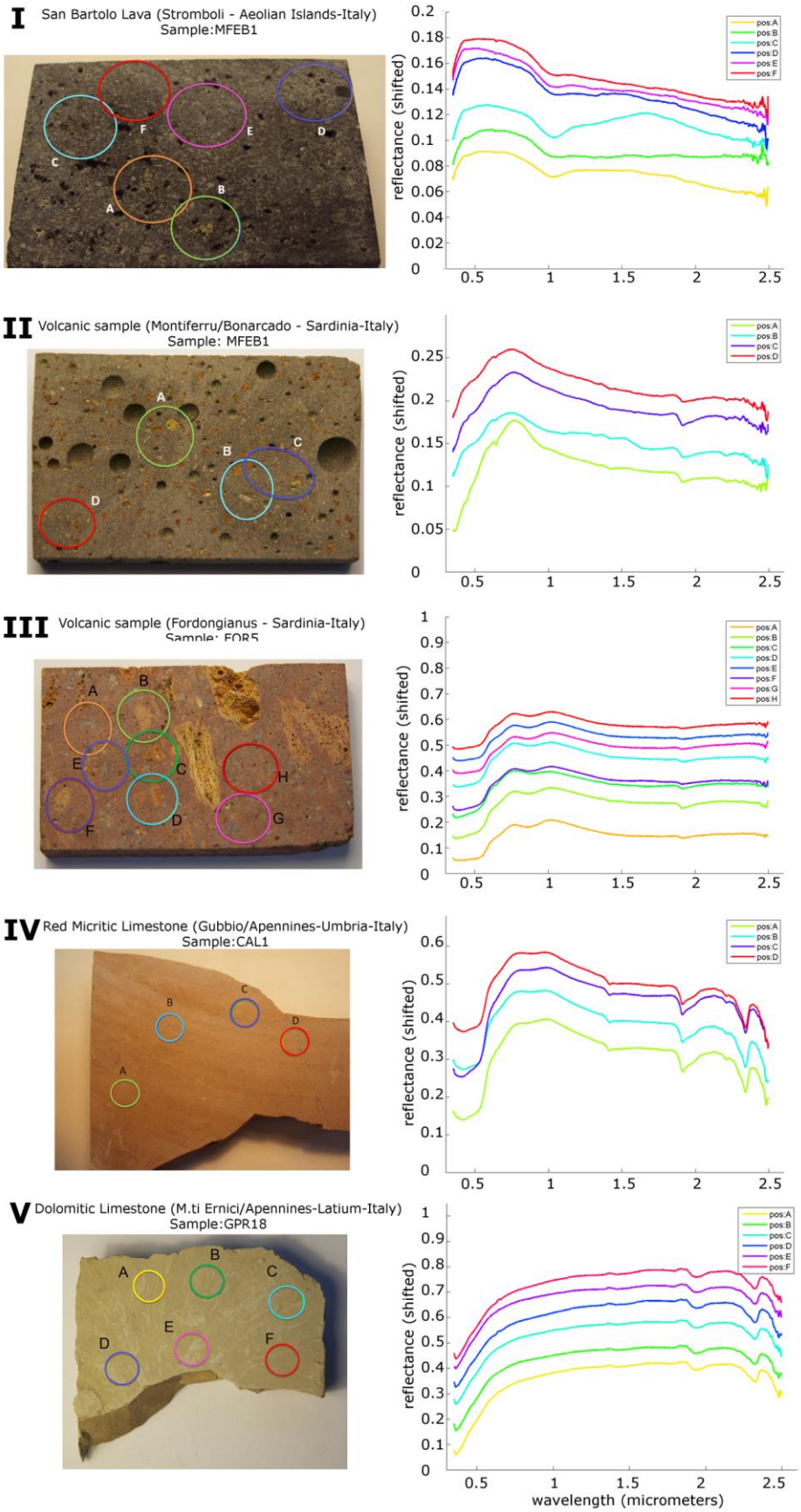

Fig.7. Spectra acquired with Spectro-Goniometer setup. I: San Bartolo Lava (STR72). II: lava from Montiferru/Bonarcado (MFEB1). III: sample from Montiferru/Fordongianus (FOR5). IV: Red micritic limestone (CAL1). V: limestone from Ernici Mountains (GPR18).

4.1.1 San Bartolo lava (STR72)

Six areas have been analyzed with the SPG setup on the surface of the San Bartolo sample (fig.7-I). One single spectrum has been acquired for each area from A to F. All spectra are characterized essentially by the crystal field (CF) absorption within Fe^{2+} at 1 μm (Burns, 1993) and by a net negative ("blue") slope in the IR. Spectra in positions B, E and F are nearly flat in the NIR range, although E and F show an absorption at 1 μm; the spectrally dominating mineralogy could be pyroxenes with iron oxides/sulfides that are responsible of very low reflectance. Spectra in positions A, C and D also show a 1-μm absorption whose right shoulder extends towards longer wavelengths, up to 1.7 μm: this could be indicative of a mixture of pyroxenes with olivine. Spectra A, C and D moreover show the Fe^{2+} absorption at 2 μm typical of pyroxene. The weak feature appearing at 0.5 μm in spectra A and B is related to spin forbidden transitions in Fe^{2+} in pyroxenes (Klima et al., 2007; Cloutis and Gaffey, 2009). However a continuum removed study would permit more quantitative analyses.

4.1.2 Lava from Montiferru/Bonarcado (MFEB1)

Spectra with SPG setup have been acquired in four areas on the surface of the Montiferru/Bonarcado sample (fig.7-II). They are all characterized by a blue slope in the IR; a weak Fe^{2+} absorption at 1 μm is superimposed onto the negative continuum in spectra A and B. Spectra C and D do not show evident CF absorptions, although a continuum removed investigation could highlight weak absorptions at 1 μm. Spin-forbidden transitions appear in the visible near 0.5 μm (probably Fe^{2+}) and in the range 0.44-0.45 μm (Fe^{2+}, Cr^{3+} or Ti^{3+}) (see Klima et al., 2007) (fig.8A). All spectra show the signs of aqueous alteration, with OH^- and H_2O overtone absorptions near 1.4 and 1.9 μm. A weak feature appears near 2.21 μm, that could be attributed to Al-OH vibrational transitions (fig.8B) (see for example Clark et al., 1990). The broad band at 1.7 μm that appears in the spectrum B could also be due to Al-OH (see for example Clark et al., 1990).

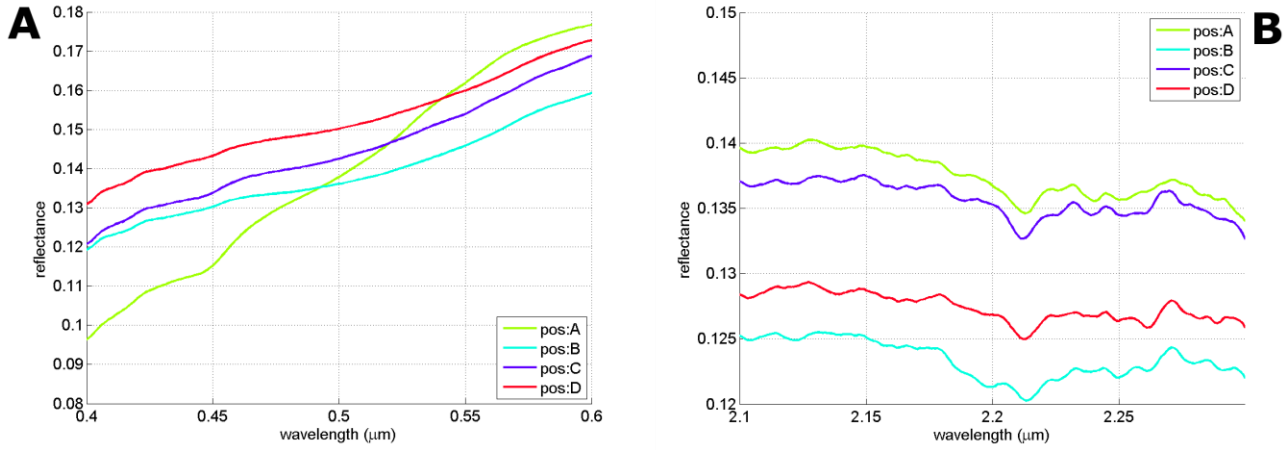

Fig.8. Sample from Montiferru/Bonarcado (MFEB1). A: electronic transitions in the VIS range. They are due to Fe^{2+} (0.5 μm) and other transition elements. B: absorption band at 2.21 micron: it is due to Al-OH vibrational transition.

4.1.3 Lava from Fordongianus (FOR5)

The eight spectra measured on the surface of FOR5 sample (fig.7-III) have very similar shapes, although there are substantial differences in the reflectance level. The main absorption features are the H_2O band at 1.9 μm, indicating some water content in the sample, and the band at 0.86-0.90 μm due to iron oxides/hydroxides (Laporte-forbidden transition in hematite/goethite Fe^{3+} ions; fig.9) (Morris et al., 1985; Clark 1999). Both these features could be indicative of chemical weathering of the sample. All spectra show a net blue slope.

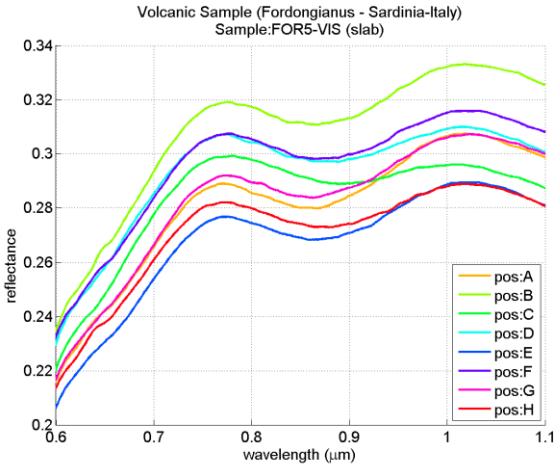

Fig.9. Sample from Montiferru/Fordongianus (FOR5). The absorption feature near 0.87-0.90 μm is likely due to Fe^{3+} transition.

4.1.4 Red micritic limestone (CAL1)

The spectra, acquired in four different areas, are similar, although with slightly different levels of absolute reflectance (range 46-50%), and with a negative slope (fig.7-IV). Spectra are characterized by CO_3^{2-} absorption bands located at 2.2 and 2.34 μm (Hunt, 1977; Gaffey, 1986; Clark et al., 1990), OH^- feature at 1.4 μm and the H_2O feature at 1.9 μm. Absorptions occurring at 0.9 μm are likely due to CF transitions within ferric ions (Fe^{3+}, fig.10) (Morris et al., 1985; Clark 1999).

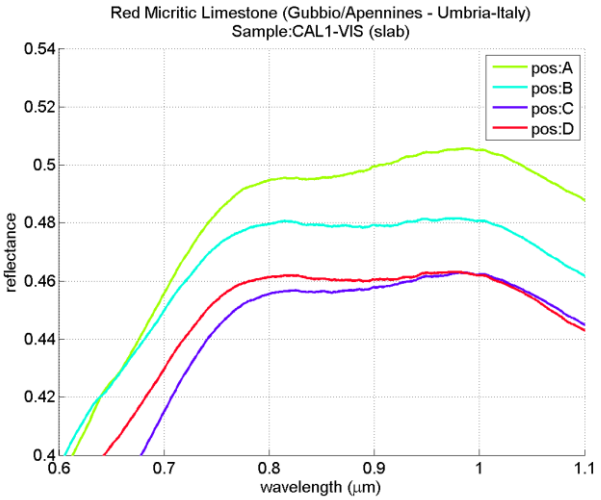

389

390 *Fig.10. Red Micritic Limestone (CAL1). The absorption feature near 0.87-0.90 μm is likely due to* Fe^{3+}
391 *transition.*

392

393 ### *4.1.5 Limestone from Mt Ernici (GPR18)*

394 The spectra of this limestone (fig.7-V; spectra shifted for clarity) are all very similar, both in
395 overall shape and in reflectance value: the maximum reflectance is about 0.55-0.60.
396 Absorption bands diagnostic of carbonate ion CO_3^{2-} appear at 1.75 and 2.34 μm (Gaffey, 1986,
397 1987); the feature at 2.2 μm is very weak and discernible only in spectrum of position F.
398 Hydroxyl and water absorptions occur at 1.4 and 1.9 μm respectively.

399

400

401

402

403

404

405

406

407

408

409

4.2 Measurements with Ma_Miss Breadboard

4.2.1 San Bartolo lava (STR72)

Spectra (fig.12-A) acquired with Ma_Miss BB within area A (fig.7-I area A) show different mineralogical phases. An example of the spots acquired with Ma_Miss within an SPG area is shown in fig.11. Absorptions at 0.9 μm (Fe^{3+}) and 1 μm (Fe^{2+} in pyroxenes) are visible in spectra in positions 1, 3 and 5. Spectra in positions 4 and 7 don't show absorptions, indicating dark/opaque materials. Spectra within area B (fig.12-B) show the presence of olivine, with a broad absorption band centered near 1 μm and extending up to 1.7 μm (positions 1,2,3). Other spectra are indicative of dark materials. In fig.12-C spectra that are indicative of pyroxene are shown, related to area C; they are characterized by pronounced absorptions at 1 and 2 μm; spectra in positions 2 and 8 also show a broad feature at 0.8 μm (CF in Fe^{3+}). Spectra acquired within area D are shown in fig.12-D. Some of them are only characterized by a faint absorption band at 1 μm, while others are spectrally flat and with variable slope. In particular spectra 1 and 4 in pos.D show a constant positive slope, differently from all other spectra of volcanics. Flat and featureless spectra are related to the black iron oxide inclusion (see fig.7-I area D). A small and narrow feature appearing near 0.6 μm in all STR72 spectra is due to an instrumental artifact.

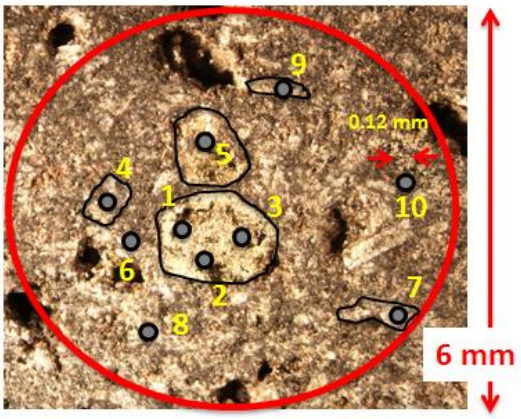

Fig.11. comparison between the spot of the SPG (6 mm, red circle) and the spot of Ma_Miss BB (0.12 mm, black-grey circles, numbered from 1 to 10); the sample is STR72, area A (see spectra in fig.12-A). Black irregular contours are traced to highlight some macroscopic features investigated with Ma_Miss BB.

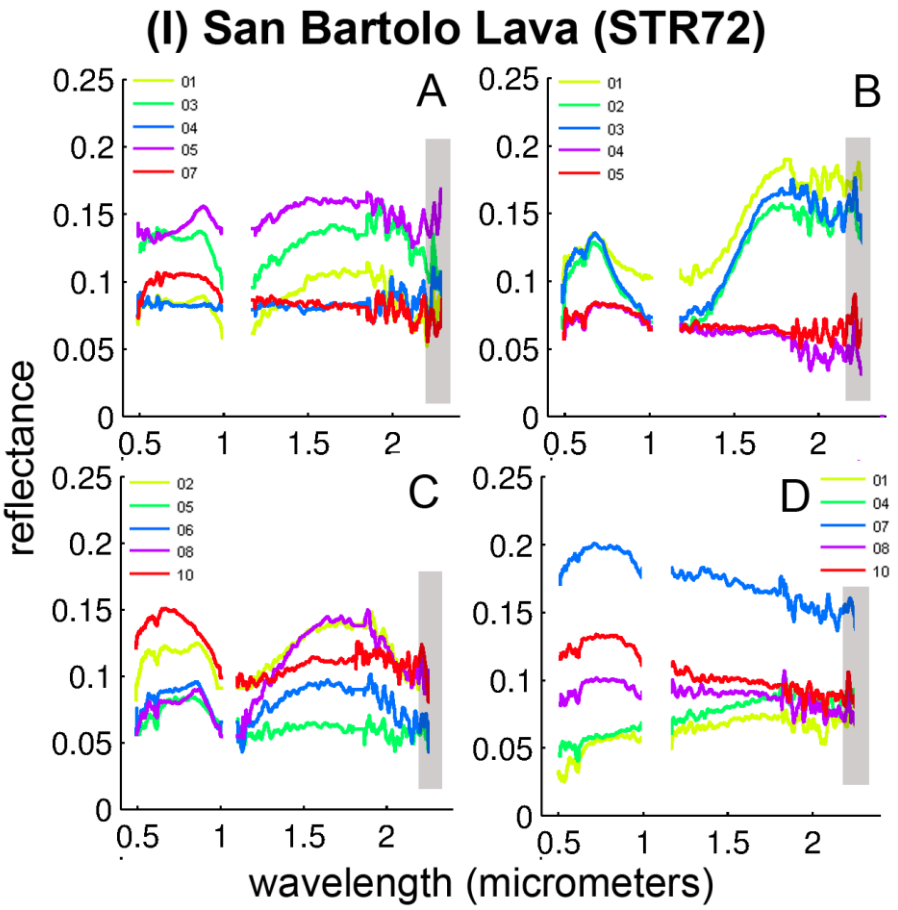

Fig.12. Spectra acquired with Ma_Miss BreadBoard setup. Sample I: San Bartolo Lava (STR72). The letters (A,B,C,D) correspond to the areas analysed with Spectro-goniometer setup (fig.2). In each single 6-mm-sized area, ten spectra in different positions have been acquired with Ma_Miss BB setup; here only five spectra are shown for clarity. Data at 1 μm are not shown in several spectra due to high level of detector noise, as well as data at λ<0.5 μm and λ>2.3 μm in some cases. Gray bars highlight the spectral region which is not accessible for Ma_MISS.

4.2.2 Lava from Montiferru/Bonarcado (MFEB1)

Spectra in fig.13-A (relative to area A in fig.7-II) show a great diversity, indicating several different mineralogical phases within the observed area. Spectra 2 and 3 (blue and green lines), with spin-forbidden absorptions at 0.65 μm (Fe^{2+}/Fe^{3+} or Ti^{3+}, see for example Clark et al., 1990, Klima et al., 2007), CF at 1 μm (Fe^{2+}), vibrational overtones at 1.4 μm (OH^-) and 1.9 μm (H_2O) are indicative of hydrated silicate minerals. A feature at 2.2 μm in spectrum 3 could be attributed to Al-OH absorption, suggesting the presence of montmorillonite or other alteration phases associated to plagioclases (see Clark et al., 1990); it must be stressed however that features occurring longward of 2.2 μm are not accessible for Ma_MISS flight instrument. The spectrum 10 is indicative of iron oxides (absorption at 1 μm) with some degree of hydration. Spectra 7 and 9 indicate the presence of dark/opaque minerals (oxides). Spectra of iron hydroxide goethite, characterized by Fe^{3+} absorption at 0.9 μm and OH/H_2O absorptions at 1.4-1.9 μm, are visible in several positions (fig.13: B, pos.3; C, pos.3,6; D, pos.3,5; see Clark 1999). Plagioclase feldspars are visible in spectra 5 and 7 of fig.13-B, as could be inferred by the CF Fe^{2+} absorption near 1.25-1.3 μm (see Adams and Goullaud, 1978).

The presence of silicate minerals with different OH/H_2O band intensities at 1.4-1.9 μm, indicative of various degree of hydration is evident in spectra 1,2 of fig.13-C. Dark opaque minerals are indicated by spectra in fig.13-B (4), fig.13-C (5) and fig.13-D (1, 8 and 10).

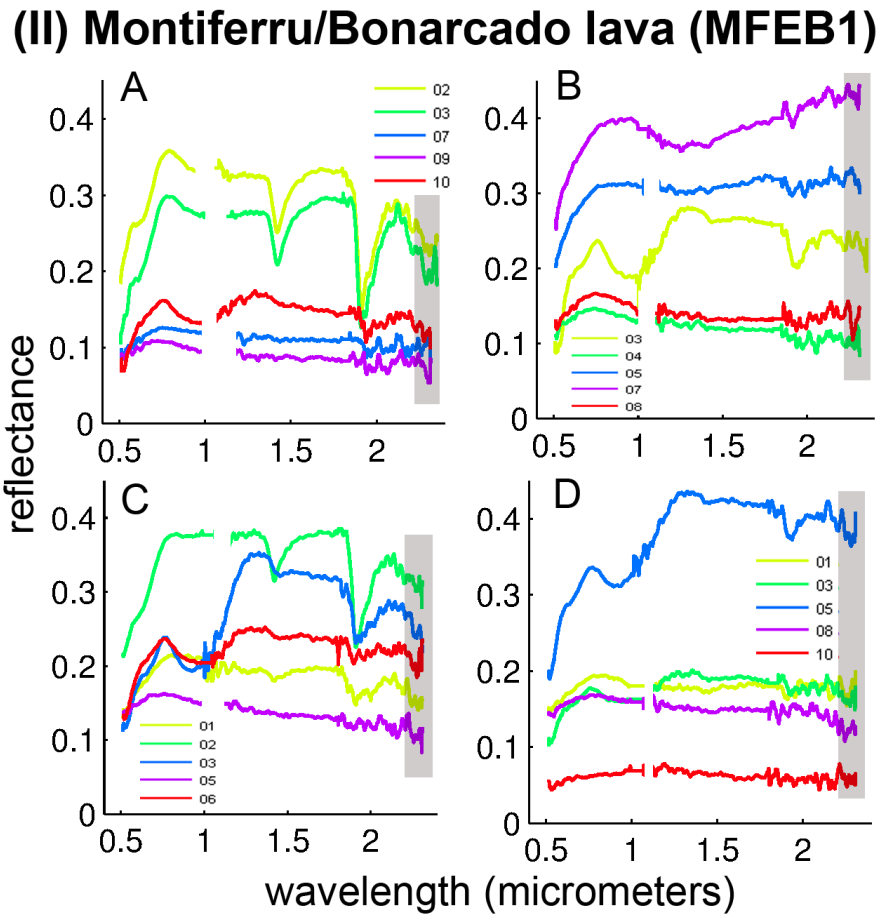

Fig.13. Spectra acquired with Ma_Miss BreadBoard setup. Sample II: Montiferru/Bonarcado Lava (MFEB1). The letters (A,B,C,D) correspond to the areas analysed with Spectro-goniometer setup (fig.2). In each single 6-mm-sized area, ten spectra in different positions have been acquired with Ma_Miss BB setup; here only five spectra are shown for clarity. Data at 1 μm are not shown in several spectra due to high level of detector noise, as well as data at λ<0.5 μm and λ>2.3 μm in some cases. Gray bars highlight the spectral region which is not accessible for Ma_MISS.

4.2.3 Lava from Fordongianus (FOR5)

Spectra are shown in fig.14. Area A (fig.14-A) is characterized by spectra similar to chert/silica, with some content of dark/opaque minerals; in some positions (spectra 5, 8 and 9) the CF Fe^{3+} absorption feature at 0.9 μm is visible (Clark, 1999). Spectra within area B (fig.14-B) are similar to chert/hydrated silica with different content of ferric iron and various degree of hydration (bands at 1.4 and 1.9 μm). Spectra relative to area C (fig.14-C) also are indicative of high-silica phases with some content of ferric iron (CF absorption in Fe^{3+}). We

must stress the point that unambiguous detection of chert/hydrated silica can be done with the diagnostic Si-OH feature located beyond 2.2 μm. Area D (fig.14-D) is characterized by the presence of hydrated minerals-iron oxide mixture (spectra in position 5,6,7 with intense OH/H_2O absorptions at 1.4-1.9 μm and CF Fe^{3+} absorptions at 0.9 μm), and by Fe^{3+}-bearing high-silica phases (pos.3,7). Al-OH alteration phases could be present in area C (pos.3) and area D (pos.3, 10) as suggested by the absorption at 2.2 μm; also in this case it must be highlighted that features appearing beyond 2.2 μm will not be observed from Ma_MISS flight instrument, and Al-OH absorptions occurring at 2.2 μm can be hardly identified.

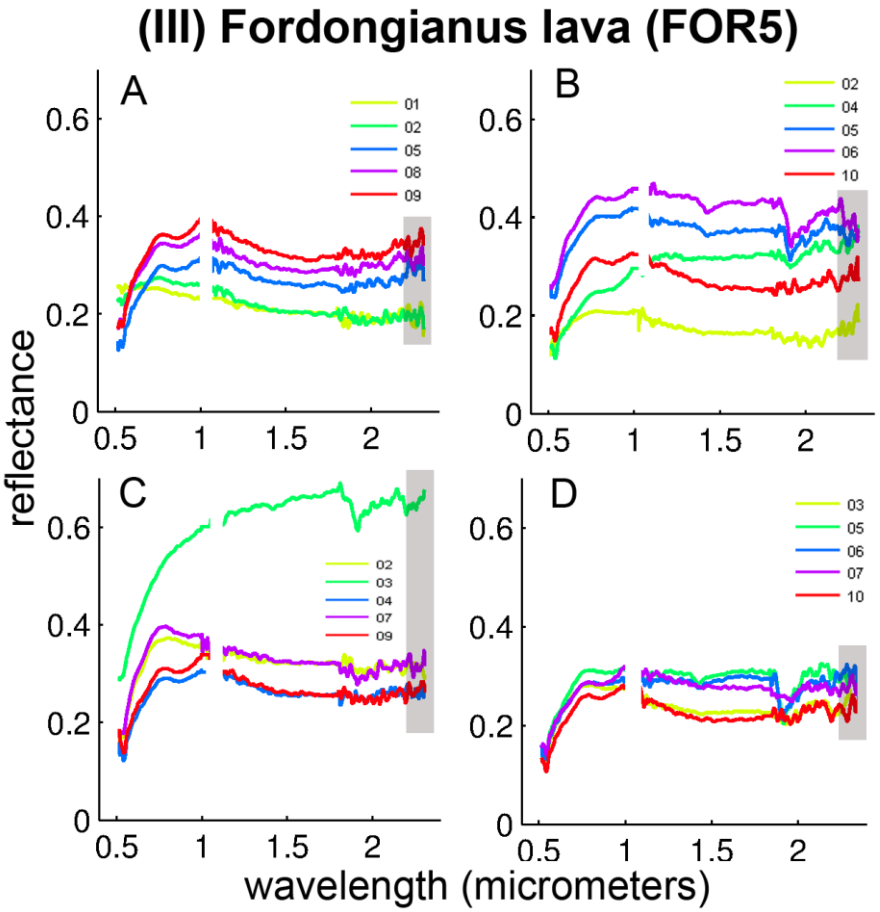

Fig.14. Spectra acquired with Ma_Miss BreadBoard setup. Sample III: Fordongianus Lava (FOR5). The letters (A,B,C,D) correspond to the areas analysed with Spectro-goniometer setup (fig.2). In each single 6-mm-sized area, ten spectra in different positions have been acquired with Ma_Miss BB setup; here only five spectra are shown for clarity. Data at 1 μm are not shown in several spectra due to high level of detector noise, as well as data at $\lambda<0.5$ μm and $\lambda>2.3$ μm in some cases. Gray bars highlight the spectral region which is not accessible for Ma_MISS.

4.2.4 Red micritic limestone (CAL1)

Spectra acquired in all positions on the micritic limestone sample are quite homogeneous, with very few differences (fig.15). All spectra are characterized by the CO_3^{2-} absorptions at 2.2 and 2.35 μm, although the noise is high in this spectral region (which is not accessible from Ma_MISS flight instruments); OH^- and H_2O bands are present at 1.4 and 1.9 μm. Spectra acquired on grey calcite veins appear relatively flat and with a blue slope (area B, pos.7,10; area C, pos.8,10; area D, pos.5,8). Spectra acquired in positions corresponding to the red micritic matrix show the CF Fe^{3+} absorption at 0.9 μm (Clark, 1999), due to some mixing of calcium carbonate with iron oxide, and a net change in slope at wavelengths shorter than 1.4 μm. It must be noted that eventual carbonates identification by Ma_MISS spectra will not be based upon features occurring in the 2.2-2.5-μm region. Eventual CO_3^{2-} absorptions appearing in the 2.16-2.2-μm region could be identified. Nevertheless the identification should be based also on the comprehensive analysis of other spectral features, such as the reflectance level, the appearing of hydration features at 1.4-1.9 μm and their shape, the occurrence of CO_3^{2-} absorptions in the 1.75-2.00-μm range, the spectral behavior in the VIS range.

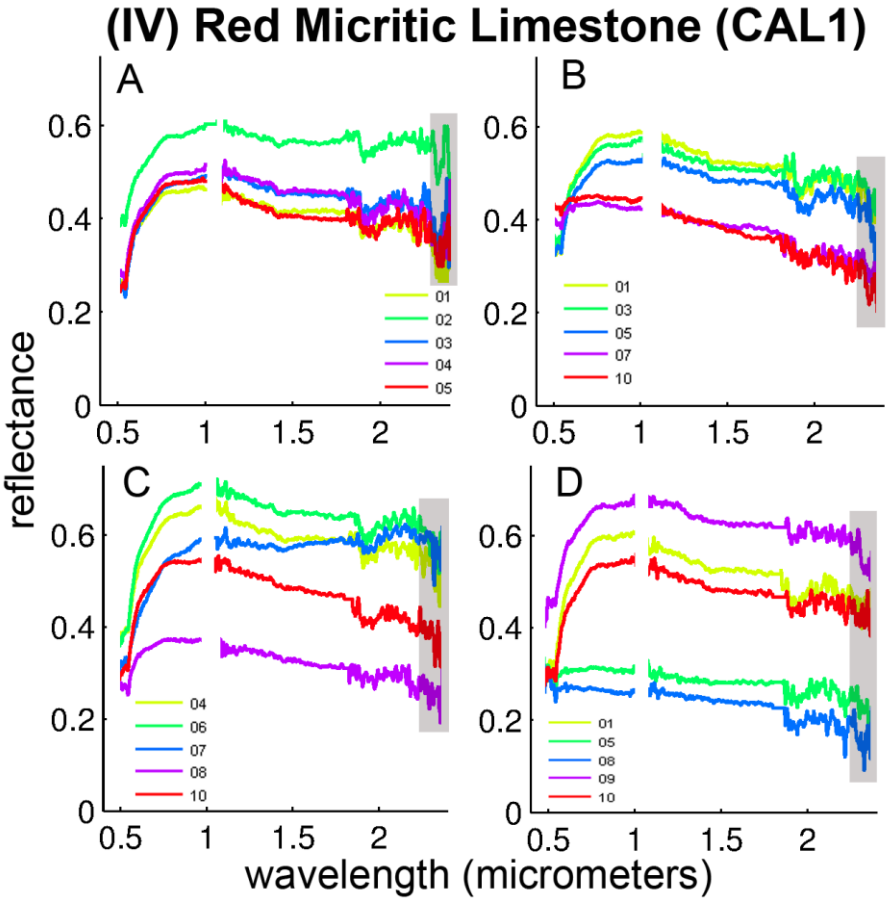

Fig.15. Spectra acquired with Ma_Miss BreadBoard setup. Sample IV: Red Micritic Limestone (CAL1). The letters (A,B,C,D) correspond to the areas analysed with Spectro-goniometer setup (fig.2). In each single 6-mm-sized area, ten spectra in different positions have been acquired with Ma_Miss BB setup; here only five spectra are shown for

clarity. Data at 1 μm are not shown in several spectra due to high level of detector noise, as well as data at λ<0.5 μm and λ>2.3 μm in some cases. Gray bars highlight the spectral region which is not accessible for Ma_MISS.

4.2.5 Limestone from Mt Ernici (GPR18)

Spectra of the limestone sample GPR18 are shown in fig.16. Spectral profiles are all very similar, with flat to slightly reddened slopes, and characterized by CO_3^{2-} absorptions near 2.2 and 2.35 μm. The carbonate feature at 2.16-2.2 μm is visible in spectra showed in panel E (Gaffey, 1986; Clark et al., 1990), while in other spectra it constitutes a unique broadened band together with the one at 1.9 μm. XRD analyses show that this sample is constituted by anhydrous dolomite and ankerite, so the 1.9-μm feature can be attributed to some adsorbed water. Spectra in fig.16-A (pos.8 and 9) also show a weak feature near 0.65 μm, that could be attributed to an Fe^{3+} spin-forbidden band or to the presence of chlorophyll.

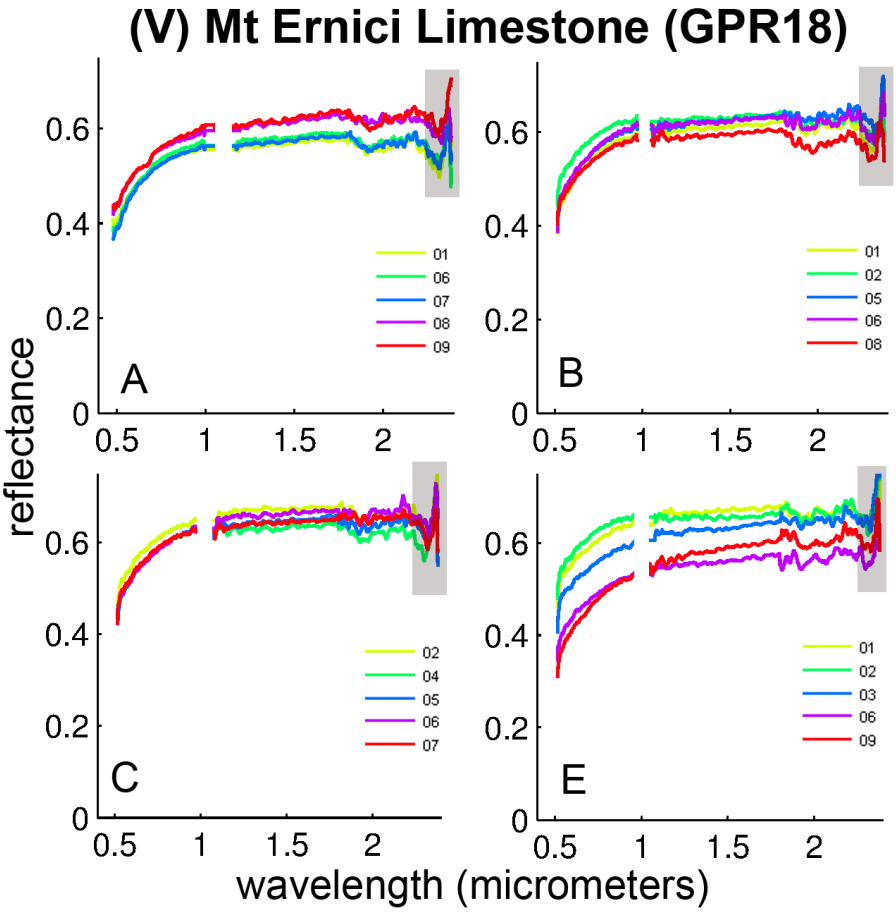

Fig.16. Spectra acquired with Ma_Miss BreadBoard setup. Sample V: Mt Ernici Limestone (GPR18). The letters (A,B,C,E) correspond to the areas analysed with Spectro-goniometer setup (fig.2). In each single 6-mm-sized area, ten spectra in different positions have been acquired with Ma_Miss BB setup; here only five spectra are shown for clarity. Data at 1 μm are not shown in several spectra due to high level of detector noise, as well as data at λ<0.5 μm and λ>2.3 μm in some cases. Gray bars highlight the spectral region which is not accessible for Ma_MISS.

5. Comparison between different spatial scales

5.1 Method 1. Average

We used arithmetic average in order to compare spectra obtained with SPG and Ma_Miss BB setup as a first method. For each sample, and for each area (A,…,D) corresponding to a SPG spectrum, the ten spectra S_i acquired with Ma_Miss BB within a zone have been averaged. The resulting mean spectrum S_{avg} is given by:

$$S_{avg} = \sum_{i=1}^{10} S_i$$

In this way all Ma_Miss spectra are considered with the same weight. In fig.17 spectra obtained after averaging Ma_Miss data (S_{avg}, blue lines) are compared with SPG spectra (S_{spg}, green lines), for each analyzed area. Each computed spectrum S_{avg} has been compared with the SPG spectrum determining the sum of residuals (standard deviation):

$$R_{avg} = \sqrt{\frac{1}{N-1}\sum_{i=1}^{N}\left(S_{avg} - S_{spg}\right)^2}$$

Generally averaged Ma_Miss spectra can reproduce quite well SPG spectra of the same areas, although some discrepancies arise. The larger discrepancy between SPG and Average are where the sample is highly heterogeneous. It must be recalled that the ten Ma_MISS spectra acquired within the SPG spot, are selected choosing the points where differences are visible from a visual inspection. The selection effect is clear for the results of the volcanic samples (STR72, MFEB1 and FOR5) that are characterized by high surface heterogeneity.

Concerning the sample STR72 there are some differences in spectral slope and in reflectance, and generally SPG spectra appear more flattened. Ma_Miss spectra in positions B,C show a more prominent and broad absorption at 1 μm than do SPG spectra: in the average spectra, olivine and pyroxene content constitute a major contribute, thus with the arithmetic average method they are overestimated by Ma_Miss. On the contrary SPG spectra of these areas are dominated by dark absorbing phases (magnetite, oxides). Spectral regions better approximated by Ma_Miss average spectra are the VIS (0.4-1 μm) in area B, and NIR-IR (1-2.2 μm) in area D (fig.13). SPG spectra of sample MFEB1 also appear more flattened with respect to Ma_Miss average spectra; spectra in positions B,C show greater differences in reflectance.

Ma_Miss Average spectra of areas A and D better approximate the SPG spectra, although the hydrated phases are overestimated in Ma_Miss spectra. Spectra of areas B, C preserve their spectral shapes in both datasets, but show different overall reflectance levels (fig.13). SPG and Ma_Miss average spectra of the three other samples (FOR5, CAL1 and GPR18) are very similar in shape and slope, although some shift in reflectance is evident especially for spectra in positions B,C (samples CAL1 and GPR18). Nevertheless all absorption features are visible at the same positions in both set of spectra.

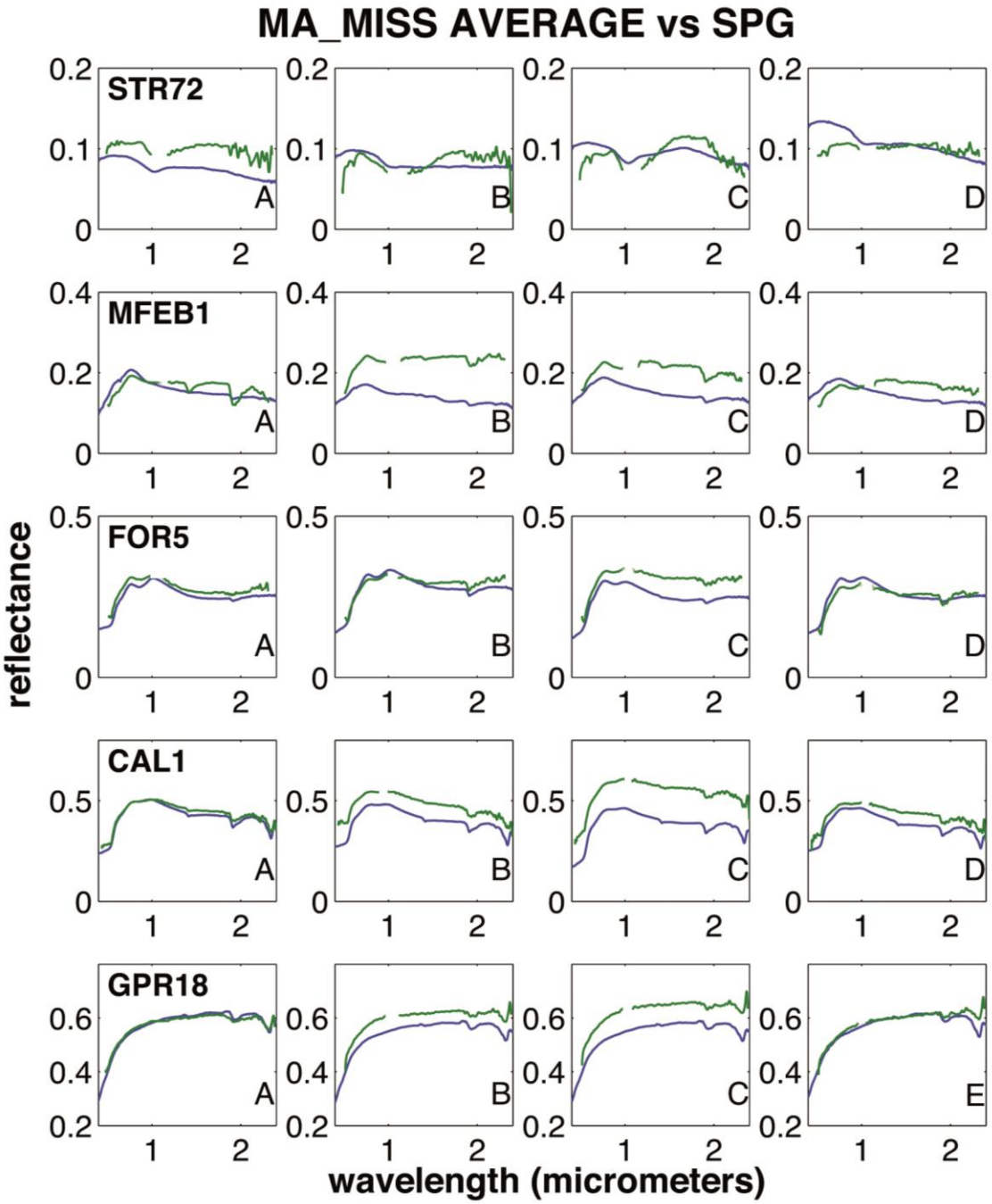

Fig.17. Comparison between SPG and Ma_Miss measurements: average spectra. Green line: Ma_Miss BB. Blue line: SPG.

5.2 Method 2. Spectral linear mixing of reflectance spectra

The second method is linear mixing of reflectance spectra. For each area analyzed on each sample, in order to compare SPG and Ma_Miss spectra, we started by choosing three endmember spectra among the ten acquired with Ma_Miss. Endmembers were chosen following two criteria: a) for the volcanic samples, spectra with marked differences in slope, shape and absorption features where chosen; b) for the carbonate samples, because no spectral differences were observed, the spectra with minimum, medium and maximum values of reflectance were chosen. Calling S_1, S_2 and S_3 the endmembers, the mixed spectrum S_{mix} is given by:

$$S_{mix} = a \cdot S_1 + b \cdot S_2 + c \cdot S_3$$

The endmembers spectra used for mixing are listed in tab.1. The parameters *a, b, c* give an estimate of the percent abundance of the selected components. The condition is that each of the parameters *a, b, c* were made to vary in the range 0-1 with steps of 0.1, and the final spectrum S_{mix} were taken in order to minimize the mean residuals:

$$R_{mix} = \sqrt{\frac{1}{N-1}\sum_{i=1}^{N}\left(S_{mix} - S_{spg}\right)^2} = \sqrt{\frac{1}{N-1}\sum_{i=1}^{N}\left(a \cdot S_1 + b \cdot S_2 + c \cdot S_3 - S_{spg}\right)^2}$$

In fig.20 the resulting minimum residual R_{mix} (red lines) are shown in comparison with R_{avg}: the formers (R_{mix}) are generally about one order of magnitude smaller than the latter ones (R_{avg}), thus indicating the goodness of this method. Looking at the spectra plotted in fig.18 we can see that the agreement between SPG and Ma_Miss mixed spectra is remarkably improved.

Concerning the sample STR72 the Ma_Miss mixed spectra (blue lines) are now characterized by reflectance values and spectral profiles very similar to SPG data. Spectra in positions B, C appear now more flattened than average spectra. The Fe^{3+} absorption at 0.9 μm appears in Ma_Miss spectra in position A, in both cases, while it doesn't appear in SPG spectra. The narrow feature appearing at about 0.65 μm in Ma_Miss spectra is an instrumental artifact.

Regarding the sample MFEB1 the overall spectral profiles are mutually consistent, although SPG spectra are characterized by a peak in the visible with higher reflectance, and are generally more flattened. The absorptions at 1.0 and 1.9 μm are well visible in both spectra.

Concerning the other three samples (FOR, CAL1 and GPR18) there is a very good agreement between the two methods (fig.18). SPG and Ma_Miss mixed corresponding spectra overlap almost entirely, with absorption features also appearing in the same positions. Very minimal differences in reflectance arise for sample FOR5 (pos.D, below 1.0 μm) and for CAL1 (pos.C,D, below 1.0 μm). Carbonate CO_3^{2-} features visible in SPG spectra of CAL1 and GPR18 in the 1.9-2.3-μm region are well approximated by Ma_Miss linear mixing spectra.

608 The linear mixing resulting parameters *a, b, c* are listed in tab.1. They provide an estimate of
609 the abundances of major components constituting the analyzed samples, although the result
610 depends on the choice of the endmembers. For example, in the sample STR72 area B, the
611 endmember n.3 (olivine; see spectra in fig.12) has an estimated abundance of 10%, while the
612 endmember 6 (dark opaque material) has an estimated abundance of about 80%. The mixed
613 spectrum of area C is instead dominated by pyroxene mineralogy (see for example
614 endmember spectra n.2 and n.10 in fig.12).

615

616

Ma_Miss spectra endmembers					$S_{MIX-REFL} = a*S_1 + b*S_2 + c*S_3$		
sample:	STR72	*Endmember spectrum number*			a	b	c
	area A	2	5	10	0.3	0.1	0.3
	area B	3	6	9	0.1	0.8	0.2
	area C	1	2	10	0.2	0.2	0.5
	area D	1	6	7	0.1	0.3	0.4
sample:	MFEB1						
	area A	2	7	10	0.1	1.0	0.1
	area B	1	4	6	0.1	0.6	0.1
	area C	2	3	10	0.1	0.1	0.5
	area D	1	5	7	0.1	0.1	0.7
sample:	FOR5						
	area A	1	2	4	0.1	0.2	0.6
	area B	4	6	10	0.1	0.1	0.8
	area C	2	6	10	0.6	0.1	0.1
	area D	3	5	7	0.5	0.1	0.4
sample:	CAL1						
	area A	1	2	9	0.7	0.1	0.2
	area B	3	4	7	0.6	0.1	0.1
	area C	5	7	8	0.2	0.1	0.6
	area D	8	9	10	0.3	0.2	0.4
sample:	GPR18						
	area A	1	4	9	0.4	0.1	0.5
	area B	6	7	8	0.3	0.5	0.1
	area C	6	8	10	0.1	0.1	0.7
	area E	2	4	8	0.5	0.1	0.4

617

618 *Tab.1. Selected Ma_Miss spectra endmembers for linear mixing; spectra are shown in fig.12-16. Final parameters*
619 *a,b,c of linear mixing are also shown.*

620

621

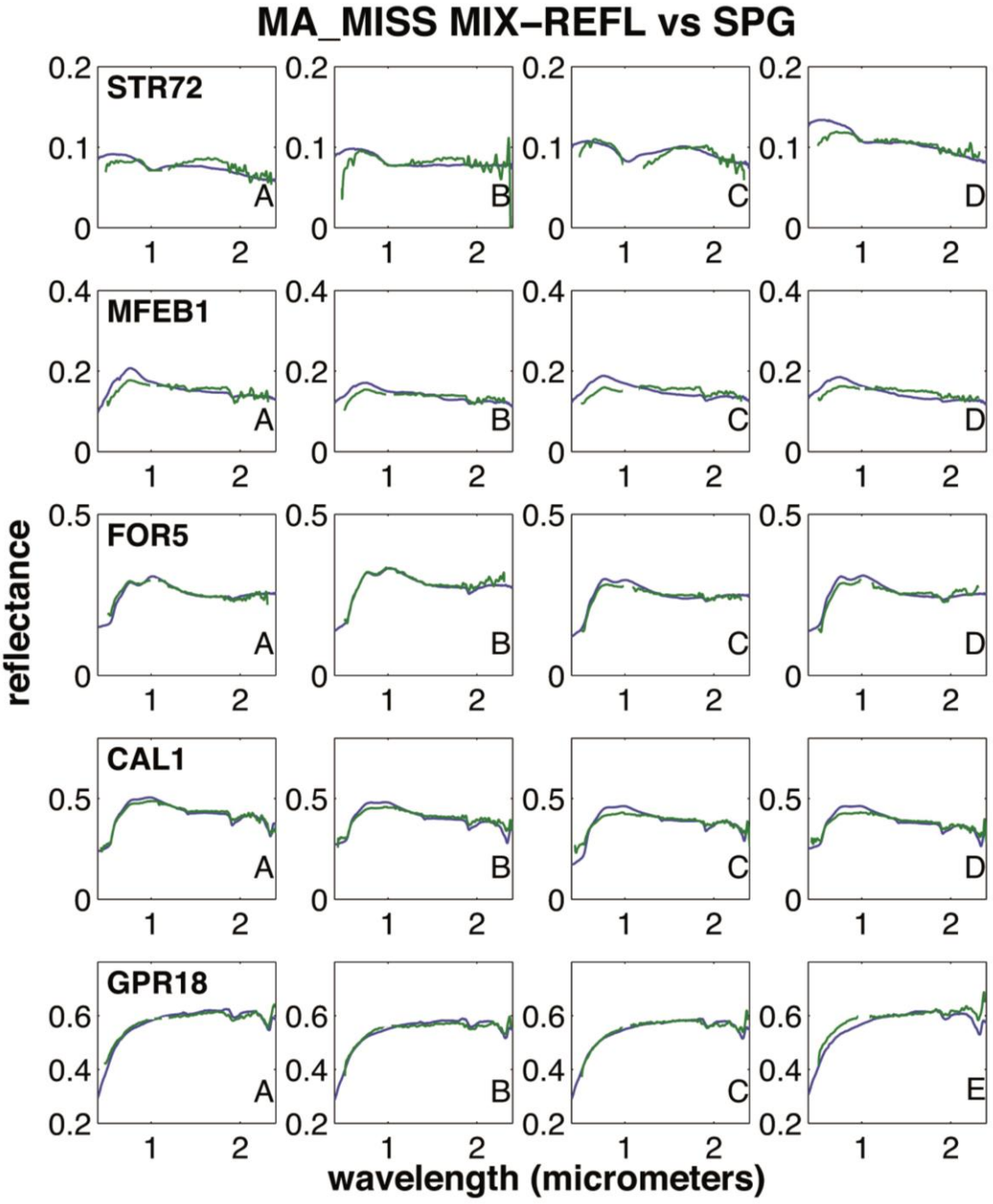

Fig.18. Comparison between SPG and Ma_Miss measurements: spectral linear mixing of reflectance spectra. Green lines: Ma_Miss BB. Blue lines: SPG.

5.3 Method 3. Spectral linear mixing of Single-Scattering Albedo spectra

A third method has been used to compare Ma_Miss and SPG spectra. Single-Scattering Albedo have been computed and then compared from both dataset. The use of SSA-spectra instead of reflectance spectra is valid in the case of microscopic mixing scale, whereas the direct combination of reflectance spectra is correct in the approximation of macroscopic mixing scale.

In this approach the SSA spectrum w corresponding to SPG measurements is first derived, using the relation:

$$R(i,e,g) = \frac{w}{4(\mu+\mu_0)} \times \left[\left(1+B(g)\right)\cdot P(g) + H(\mu)H(\mu_0) - 1\right]$$

In which R is the measured reflectance, i and e are the incidence and emission angles respectively, μ=cos(e) and μ_0=cos(i) [Mustard and Pieters, 1987 adapted from Hapke, 1981]. Under some assumptions, namely (i) grain sizes >> wavelengths, (ii) *i,e* = 15-40°, (iii) particles compacted and scattering light isotropically, the above relation can be simplified (Mustard and Pieters, 1987). It must be highlighted that here we apply the Hapke model to slab surfaces, while in previous works, this model is typically applied to particulate minerals measured in laboratory (for example Mustard and Pieters, 1987) or to remote-sensing data (Ciarniello et al., 2011). Details on the calculation are provided in the on-line Supplementary Material. The simplified equation is:

$$R = \frac{w}{4(\mu+\mu_0)} \times \left(\frac{1+2\mu}{1+2\mu\gamma}\right) \times \left(\frac{1+2\mu_0}{1+2\mu_0\gamma}\right)$$

Subsequently the SSA spectra of the Ma_Miss endmembers spectra (the same as in section 4.5) have been computed. The linear mixing of Ma_Miss endmembers SSA spectra is given by:

$$w_{mix} = a\cdot w_1 + b\cdot w_2 + c\cdot w_3$$

and the optimal parameters *a,b,c* have been derived by minimizing the relation:

$$R_{mix} = \sqrt{\frac{1}{N-1}\sum_{i=1}^{N}\left(w_{mix} - w_{spg}\right)^2}$$

The derived parameters are listed in tab.2, and the Ma_Miss SSA spectra w_{mix} are compared with SPG SSA spectra w_{spg} in fig.19. They show very good agreement for the two carbonate samples (CAL1 and GPR18) and the volcanic sample FOR5. Concerning the CAL1 and GPR18 carbonate samples, the CO_3^{2-} absorptions in the 1.9-2.3-μm region are well represented in the Ma_Miss linear mixing SSA spectra. Absorptions at 0.9 μm related to Fe^{3+} in FOR5 sample are visible in SPG spectra and well approximated by Ma_Miss linear mixing spectra for almost all areas. The albedo values are mutually consistent along the overall spectral range for these three samples. The matching is less good for the other two volcanic samples, MFEB1 and especially STR72. This is due to differences in the albedo of the samples as well as in the

spectral shape in the 1.2-2.2-μm region. Deviations between the two methods appear also for wavelengths λ<0.7 μm, especially for STR72. While the two carbonates and FOR5 have moderately high levels of albedo, the sample MFEB1 has a moderately low level of reflectance, and STR72 is very dark: the assumptions and approximate equations used here are valid for albedo >10%, when materials don't behave like strong absorbers (i.e. in absence of very strong iron absorptions) (Mustard and Pieters, 1987).

This conclusion is further highlighted in fig.20, in which the residuals derived with the three methods are compared. Regarding the samples CAL1 and GPR18 the residual $R_{mix\text{-}SSA}$ is generally less than $R_{mix\text{-}REFL}$ and R_{avg}, while for the volcanic samples FOR5 and MFEB1 we have $R_{mix\text{-}REFL} < R_{mix\text{-}SSA} < R_{avg}$. Finally the highest values of $R_{mix\text{-}SSA}$ are obtained for the darkest sample STR72.

$w_{MIX\text{-}SSA} = a*w_1 + b*w_2 + c*w_3$				
		a	b	c
sample:	STR72			
	area A	0.2	0.1	0.5
	area B	0.2	0.6	0.2
	area C	0.1	0.3	0.5
	area D	0.1	0.4	0.4
sample:	MFEB1			
	area A	0.1	0.9	0.1
	area B	0.1	0.6	0.2
	area C	0.3	0.1	0.4
	area D	0.1	0.2	0.6
sample:	FOR5			
	area A	0.1	0.5	0.4
	area B	0.1	0.1	0.8
	area C	0.7	0.1	0.1
	area D	0.7	0.1	0.2
sample:	CAL1			
	area A	0.8	0.1	0.1
	area B	0.1	0.1	0.8
	area C	0.1	0.2	0.7
	area D	0.3	0.1	0.6
sample:	GPR18			
	area A	0.6	0.1	0.3
	area B	0.1	0.1	0.8
	area C	0.1	0.1	0.8
	area E	0.5	0.1	0.4

Tab.2. Linear mixing of Single-Scattering Albedo spectra, final parameters a, b, c.

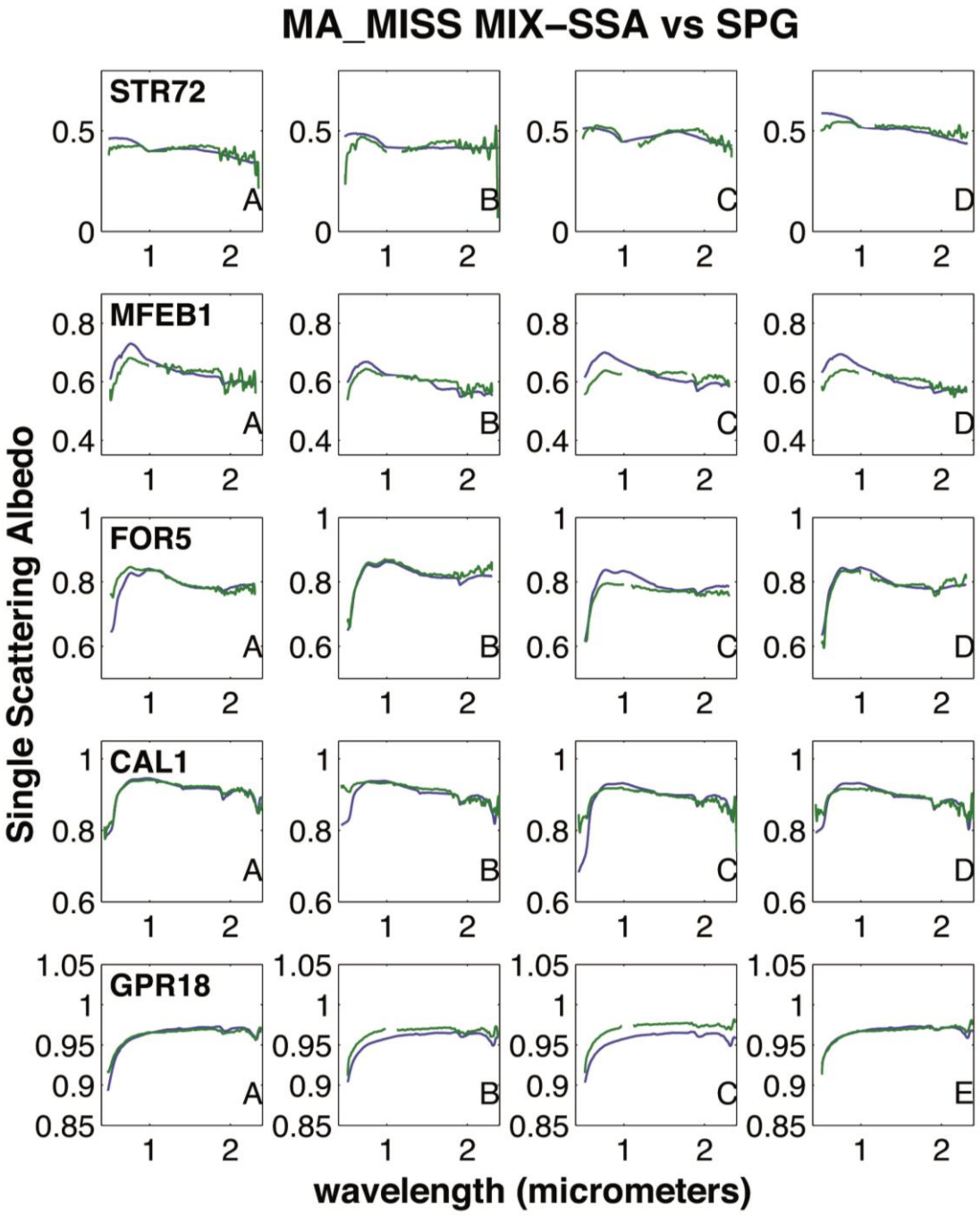

Fig.19. Comparison between SPG (blue lines) and Ma_Miss (green lines) measurements: spectral linear mixing of Single Scattering Albedo (SSA) spectra.

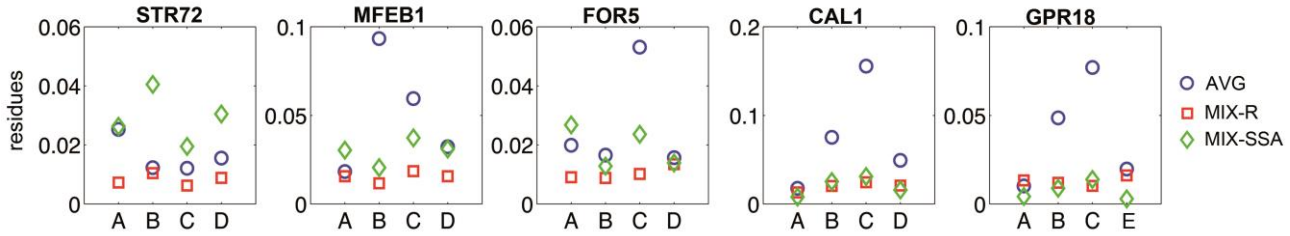

682

683 *Fig.20. Sum of residuals computed by comparing SPG spectra and Ma_Miss BB spectra, obtained by (i) averaging*
684 *(blue diamonds), (ii) using linear mixing of reflectance spectra (red squares), (iii) using linear mixing of Single-*
685 *Scattering Albedo spectra (green diamonds). On X-axes the letters corresponding to analyzed areas are indicated.*

686

687 # 6. Discussion

688 *Differences between the two instruments and spatial scales*

689 Analyses of the five rock slabs (three volcanic and two carbonate samples) with Spectro-
690 Goniometer setup permitted to determine their bulk spectral composition at a scale >1
691 mm, given the SPG spot size of about 6 mm. This analysis allows to obtain an overall
692 information about the average spectral behavior of the samples; it takes advantage in that
693 it is useful in order to provide a first immediate approximate characterization of a rock
694 sample in terms of average absorptions, spectral slopes, reflectance level; in principle this
695 could be helpful in assign a sample to a macro-category of rocks (volcanic, sedimentary,
696 etc.). Nevertheless on the other side the analyses performed with this setup are not able to
697 provide, for example in a volcanic sample, suitable information to discriminate between
698 groundmass and phenocrysts or xenoliths. The large acquisition spot generally includes
699 many different mineralogical phases and cannot help in discriminating among surface
700 heterogeneity at smaller scale.

701 Analyses performed using the Ma_Miss BreadBoard setup result in a major improvement
702 in the capability of investigate the surface heterogeneity of the rocks. The smaller spot size
703 obtainable thanks to the coupling of Ma_Miss Optical Head and fiber (120 μm) allowed to
704 perform spectral investigation of rocks surfaces at one tenth of millimeter-scale, thus
705 getting information on inclusions and mineral grains of the order of hundred micrometers
706 in size. Analysis of volcanic porphyritic samples with this spatial resolution could in
707 principle permit to spectrally distinguish the rock groundmass from
708 phenocrysts/xenoliths or lithic clasts. Spectral study of igneous holocrystalline plutonic
709 rocks allows to discriminating among the different mineral crystals, thus evaluating the
710 surface heterogeneity in great detail and getting clues about mineralogical diversity.

711 Ma_MISS high spatial resolution also proves to be able to resolve a greater number of
712 minerals than what resolved by the 6-mm resolution Spectro-Goniometer. A good point is
713 for example the identification of plagioclase grains (fig.13B, spectrum #7) within the lava
714 sample from the Montiferru (MFEB1). Plagioclases are typically difficult to be detected
715 with spectroscopy especially in the VNIR range and when they are embedded in a matrix
716 with more spectroscopically active minerals.

Applicability of Hapke model to bulk rock slabs

The application of Hapke model to bulk rock slabs spectra must be somewhat discussed. The Hapke model (Hapke, 1981, 1993) has been fundamentally developed in order to explain the optical behavior of particulate materials, typically compact/loose powders (i.e. planetary regoliths) or atmospheres, and in that sense has been widely applied by many authors. When this model is applied to bulk rock slabs some differences with respect to particulate must be taken into account.

Widely dispersed particles can be treated as a continuum medium, in which no interferences arise between light rays propagating among particles, and grains don't cast shadows on each other. When particles get more closely packed each other or they are in contact, the medium can no longer be considered as continuum. Interferences arise between portions of waves scattered by adjacent grains; nevertheless for irregular shaped and random oriented particles all coherent effects will be averaged and erased (Hapke, 1981).

Moreover while in a widely dispersed particulate medium, in which particles are $d>>\lambda$ in size, diffraction cannot be neglected (it's related to forward-scattering), in closely-packed or contact grains the diffraction becomes meaningless and undistinguishable from light scattered by other adjacent particles.

Another aspect is that in a widely disperse particulate medium each single grain is fully illuminated and the scattering/absorption efficiencies are full quantities. In a medium in which interstices are small (compacted powder or bulk rock) the particle cross sections are reduced by other particles' shadows. This implies that scattering and absorption efficiencies are all reduced by the same factor. Anyway their ratios (in w and $P(g)$) in principle remain unchanged.

It is to be considered that within a slab the optical coupling between grains is different with respect to a powder: while relative refraction indexes at grain boundaries in a powder are typically mineral/air or mineral/vacuum, relative refraction indexes within a slab are mineral/mineral (Hapke, 1993). This different optical coupling causes surficial reflections at grain boundaries to be reduced, thus implying a variation in Q_S (*scattering efficiency*) and $p(g)$. Forward scattering dominates in optically thin grains within a slab (Hapke, 1993), which in turn results darker than separate grains. As a consequence optical properties of bulk rock/slabs are somewhat different with respect to properties of separate minerals extracted from the bulk rock: optical parameters obtained are somewhat different in the two cases, nevertheless equations are still applicable.

Comparison of the three methods and endmember retrieval

The first method used to combine Ma_Miss spectra consisted in averaging all measured spectra. Although this results in a good first order approximation to reproduce SPG spectra, nevertheless it is imperfect. The arithmetic average of all measured spectra within

a zone results in all spectra having the same statistical weight. The spectra measured with Ma_Miss within a zone correspond to different mineralogical phases that can show a different spectral behavior and especially can have diverse spectral weights within a mixture: more absorbing phases (e.g. iron oxides) can dominate the mixture (i.e. SPG) spectrum even if they have low abundance.

The other two methods (linear mixing of reflectances and of SSA) results in a substantial improvement and a better matching between combined Ma_Miss spectra and corresponding SPG spectrum. The linear mixing algorithm correctly takes into account the diverse spectral weight of different mineralogical phases. However in the linear mixing procedure a source of error can be manual choice of endmembers. Among the ten Ma_Miss spectra acquired within each SPG zone, three endmember spectra were visually chosen: the choice criterion was that of select the three most diverse spectra among all. Clearly this visual/manual choice of endmembers can be a source of error, because some mineralogical phases can be over/underestimated. A further general source of error can arise from the limited number of Ma_Miss spectra (ten) acquired within each SPG zone. Ma_Miss spectra were collected randomly within each zone after checking that zone both visually and using optical microscope. Clearly a higher number of Ma_Miss spectra acquired within each zone would result in a better matching, when combined and mixed, with SPG spectra. A different collection pattern of the 10 spectra within each SPG zone could give in principle a somewhat different sampling of the same area, although we would expect statistically the same results.

7. Conclusions

In this work we analyzed a set of five rock slabs by mean of VNIR spectroscopy in order to characterize the Ma_Miss instrument capability to accomplish mineral investigations. For this purpose, we used two different instruments: (i) the Spectro-goniometer setup, that is a Fieldspec Pro coupled with a goniometer, with spectral range 0.35-2.5 μm and spatial resolution spot of 6 mm; (ii) the ExoMars/Ma_Miss BreadBoard setup, with analogous spectral range and higher spatial resolution (spot of 0.12 mm).

The rock slabs were first analyzed with the Spectro-goniometer setup (SPG), acquiring spectra from few 6-mm-diameter areas on the rock surfaces; the SPG allows getting an average information on a ten-millimeter scale. Successively the analysis of the same areas by using the Ma_Miss breadboard (BB) setup, acquiring 10 spectra with increased spatial resolution within each SPG area, allowed retrieving spectral information with much greater detail, on sub-millimeter scale. The smaller spot of Ma_Miss (0.12 mm) allows recognizing different mineralogical phases with size down to about one hundred microns.

For each analyzed zone, spectra acquired with Ma_Miss at 120 μm spatial resolution were combined in different ways in order to be compared with the SPG spectrum of the same zone: (i) by arithmetic average of all ten spectra; (ii) by linear mixing of three endmember

795 refletctances; (iii) by linear mixing of three endmember Single Scattering Albedos (using
796 Hapke Model).

797 The average method provides good agreement between SPG and Ma_Miss spectra,
798 although linear mixing of endmembers reflectance spectra results in a notable
799 improvement. Further improvement is obtained when combining and comparing Single-
800 Scattering Albedo spectra instead of the reflectance. This approach is more valid and
801 rigorous in the case of microscopic mixing scale of the materials; nevertheless it shows
802 some limitation and mismatching when applied to samples that behave like very strong
803 absorbers, i.e. characterized by reflectance levels less than 10%.

804 Linear mixing, both of reflectance spectra and of Single-Scattering Albedo, of Ma_Miss BB
805 spectra resulted in an excellent agreement between mixed Ma_Miss spectra and SPG
806 spectra of corresponding areas, better than simply arithmetical averages.

807

808 ## Acknowledgements

809 We wish to thank ASI for fully supporting the Ma_Miss project (ASI GRANT n. 2015-002-
810 R.0.). We also wish to thank Alessandro Frigeri (IAPS) for having provided the red micritic
811 limestone (CAL1), and to Gianfilippo De Astis (INGV) who provided the Aeolian sample
812 (STR72) with relative chemical analyses. We are grateful to Ed Cloutis for his helpful
813 comments and suggestions.

814

815 ## References

816 Adams, J.B. and Goullaud, L.H.: *Plagioclase Feldspars: visible and near-infrared diffuse*
817 *reflectance spectra as applied to remote sensing*, Proc. Lunar Planet. Sci., Conf. 9th, pp.2901-
818 2909, 1978

819 Alvarez W.: *The historical record in the Scaglia limestone at Gubbio: magnetic reversals and*
820 *the Cretaceous-Tertiary mass extinction*, Sedimentology, 56, 137–148, doi: 10.1111/j.1365-
821 3091.2008.01010.x, 2009

822 Bibring J.P., et al.: *Perennial water ice identified in the south polar cap of Mars*, NATURE, Vol
823 428, doi:10.1038/nature02474, 2004

824 Bibring J.P., et al.: *Mars Surface Diversity as Revealed by the OMEGA/Mars Express*
825 *Observations*, Science 307, 1576, DOI: 10.1126/science.1108806, 2005

826 Boynton W.V., et al.: *Distribution of Hydrogen in the Near Surface of Mars: Evidence for*
827 *Subsurface Ice Deposits*, Science 297, 81, DOI: 10.1126/science.1073722, 2002

828 Burns, R.G.: *Mineralogical Applications of Crystal Field Theory*. Cambridge University Press,
829 Cambridge, UK, p.551, 1993

Carli C.: *Spectral Analyses in the VNIR of Igneous Rocks: Surface Composition Characterization of Terrestrial Planets*, PLINIUS, n.35, 2009

Carli C. and Sgavetti M.: *Spectral characteristics of rocks: Effects of composition and texture and implications for the interpretation of planet surface compositions*, Icarus, 211, 1034-1048, 2011

Carli C., et al.: VNIR spectral variability of the igneous stratified Stillwater Complex: A tool to map lunar highlands, American Mineralogist 99, 1834–1848, 2014

Ciarniello M. et al.: "*Hapke modeling of Rhea surface properties through Cassini-VIMS spectra*", Icarus 214, 541–555, 2011

Cita M.B. et al. (editors). *Catalogo delle formazioni. Unità tradizionali, Carta Geologica d'Italia 1:50.000*. Capitolo 2: "*Appennino, Scaglia Rossa*", a cura di Petti F.M. e Falorni P., Quaderni serie III, Volume 7, Fascicolo VI, 318 pp, 2005

Clark, R.N., et al.: *High spectral resolution reflectance spectroscopy of minerals*. Journal of Geophysical Research, 95 (B8) (12653–12680), 1990

Clark, R. N.: *Chapter 1: Spectroscopy of Rocks and Minerals, and Principles of Spectroscopy*, in *Manual of Remote Sensing, Volume 3, Remote Sensing for the Earth Sciences*, (A.N. Rencz, ed.) John Wiley and Sons, New York, p 3- 58, 1999.

Cloutis E.A. and Gaffey M.J.: *Searching For The 506-nm Pyroxene Absorption Band In Meteorite Spectra*, 72nd Annual Meteoritical Society Meeting, abstract n.5078, 2009

Coradini A., et al.: *MA_MISS: Mars Multispectral Imager for Subsurface Studies*, Adv. Space Res., Vol.28, No.8, pp. 1203-1208, 2001

Cousin A., et al.: *Compositions of coarse and fine particles in martian soils at gale: A window into the production of soils*, Icarus, 249, 22-42, 2015

De Angelis S., et al.: *The Ma_Miss instrument performance, I: Analysis of rocks powders By Martian VNIR spectrometer*, Planetary and Space Science 101, 89–107, 2014

De Angelis S., et al.: *The Ma_Miss instrument performance, II: Band parameters of rocks powders spectra by Martian VNIR spectrometer*, Planetary and Space Science 117, 329–344, 2015

De Sanctis M.C., et al.: *Ma_Miss On Exomars: Mineralogical Characterization Of The Martian Subsurface*, Astrobiology, paper accepted, 2017

Ehlmann, B.L., Edwards, C.S.: *Mineralogy of the Martian Surface*, Annu. Rev. Earth Planet. Sci. 42, 291–315, 2014

Fedele L., et al.: *The Pliocene Montiferro volcanic complex (central-western Sardinia, Italy): geochemical observations and petrological implications*, Periodico di Mineralogia, 76, 101-136, SPECIAL ISSUE: From Petrogenesis to Orogenesis, doi:10.2451/2007PM0011, 2007

865 Gaffey, S.: *Spectral reflectance of carbonate minerals in the visible and near infrared (0.35–*
866 *2.55 microns): calcite, aragonite and dolomite*. American Mineralogist, 71, 151–162, 1986

867 Gaffey, S.: *Spectral Reflectance Of Carbonate Minerals In The Visible And Near Infrared*
868 *(0.35-2.55 Um). Anhydrous Carbonate Minerals*. Journal of Geophysical Research, vol.92,
869 no.B2, pages 1429-1440, 1987

870 Gurgurewicz J., et al.: *Inferring alteration conditions on Mars: Insights from near-infrared*
871 *spectra of terrestrial basalts altered in cold and hot arid environments*, Planetary and Space
872 Science, 119, 137-154, 2015

873 Hapke, B.: *Bidirectional reflectance spectroscopy, 1. Theory*, Journal of Geophysical
874 Research, vol. 86, 3039-3054, 1981

875 Hapke, B.: *Theory of Reflectance and Emittance Spectroscopy*, Cambridge University Press,
876 doi: https://doi.org/10.1017/CBO9780511524998, Online ISBN 9780511524998, p.455,
877 1993

878 Harloff J. and Arnold G.: *Near-infrared reflectance spectroscopy of bulk analog materials for*
879 *planetary crust*, Planetary and Space Science, 49, 191-211, 2001

880 Hunt, G.R.: *Spectral signatures of particulate minerals in the visible and near infrared*.
881 Geophysics 42 (3), 501–513, 1977

882 Isaacson P.J., et al.: *The lunar rock and mineral characterization consortium: Deconstruction*
883 *and integrated mineralogical, petrologic, and spectroscopic analyses of mare basalts*,
884 Meteoritics & Planetary Science 46, N.2, 228–251, doi: 10.1111/j.1945-
885 5100.2010.01148.x, 2011

886 Klima R.L., et al.: *Spectroscopy of synthetic Mg-Fe pyroxenes I: Spin-allowed and spin-*
887 *forbidden crystal field bands in the visible and near-infrared*. Meteoritics & Planetary
888 Science 42, Nr 2, 235–253, 2007

889 Laiolo M. and Cigolini C.: *Mafic and ultramafic xenoliths in San Bartolo lava field: New*
890 *insights on the ascent and storage of Stromboli magmas*. Bulletin of Volcanology, 68,
891 pp.653-670, DOI: 10.1007/s00445-005-0040-7, 2006

892 Langevin, Y., et al.: *Summer Evolution of the North Polar Cap of Mars as Observed by*
893 *OMEGA/Mars Express*, Science, vol. 307, 5715, pp. 1581-1584, DOI: 10.1126/
894 science.1109438, 2005

895 Langevin, Y., et al.: *Observations of the south seasonal cap of Mars during recession in 2004-*
896 *2006 by the OMEGA visible/near-infrared imaging spectrometer on board Mars Express*,
897 Journal of Geophysical Research, vol. 112, E8, DOI: 10.1029/2006JE002841, 2007

898 Longhi I., et al.: *Spectral analysis and classification of metamorphic rocks from laboratory*
899 *reflectance spectra in the 0.4-2.5 μ m interval: A tool for hyperspectral data interpretation*,
900 International Journal of Remote Sensing, 22:18, 3763-3782, 2001

Longhi I., et al.: *Complex spectral interactions of different minerals and textures in Mars terrestrial analogues: Some examples*, Planetary and Space Science, 52, 141-147, 2004

Lowrie W. and Alvarez W.: *Late Cretaceous geomagnetic polarity sequence: detailed rock and palaeomagnetic studies of the Scaglia Rossa limestone at Gubbio, Italy*, Geophys. J. R. astr. SOC. 51, 561-581, 1977

Morris R.V., et al.: *Spectral and Other Physicochemical Properties of Submicron Powders of Hematite (α-Fe2O3), Maghemite (γ-Fe2O3), Magnetite (Fe3O4), Goethite (α-FeOOH), and Lepidocrocite (γ-FeOOH)*, Journal Of Geophysical Research, vol. 90, NO. B4, PAGES 3126-3144, MARCH 10, 1985

Murchie S.L., et al.: *A synthesis of Martian aqueous mineralogy after 1 Mars year of observations from the Mars Reconnaissance Orbiter*, Journal Of Geophysical Research, Vol. 114, E00D06, doi:10.1029/2009JE003342, 2009

Mustard J.F. and Pieters C.M.: *Quantitative Abundance Estimates from Bidirectional Reflectance Measurements*, Proceedings of the 17th Lunar and Planetary Science Conference, part 2, Journal of Geophysical Research, vol. 92, N.B4, E617-E626, 1987

Niles P.B. et al.: *Geochemistry of Carbonates on Mars: Implications for Climate History and Nature of Aqueous Environments*, Space Sci Rev, 174:301–328, DOI 10.1007/s11214-012-9940-y, 2013

Peccerillo, A., et al.: *Compositional Variations of Magmas in the Aeolian Arc: Implications for Petrogenesis and Geodynamics*. 37. Geological Society, London, Memoirs, pp.491–510, http://dx.doi.org/10.1144/M37.15, 2013

Pompilio L., et al.: *Visible and near-infrared reflectance spectroscopy of pyroxene-bearing rocks: New constraints for understanding planetary surface compositions*, Journal Of Geophysical Research, Vol. 112, E01004, doi:10.1029/2006JE002737, 2007

Preti G.P., et al.: *Spectrometers And Imaging Cameras For Planetary Remote Sensing*, 62nd International Astronautical Congress, IAC-11.A3.5.7, 2011

Sgavetti M., et al.: *Reflectance spectroscopy (0.3–2.5 μm) at various scales for bulk-rock identification*, Geosphere, v. 2, n. 3, p. 142–160, doi: 10.1130/GES00039.1, 2006

Vago, J.L., Kminek,G.: Putting together an exobiology mission: the ExoMars Example. In: Horneck, Gerda, Rettberg, Petra (Eds.), Complete Course in Astrobiology, (Eds.) WILEY-VCH Verlag, 2007

Vago, J.L., et al.: *ExoMars, ESA's next step in Mars exploration*. ESA Bull. Mag. 155,12–23, 2013

Vaniman D.T. et al.: *Mineralogy of a Mudstone at Yellowknife Bay, Gale Crater, Mars*, SCIENCE, VOL 343, DOI: 10.1126/science.1243480, 2014